

Transition Probability for the Neutrino Wave in Muon Decay and Oscillation Experiments

Kenzo Ishikawa⁽¹⁾, Tasuku Nozaki⁽¹⁾, Masashi Sentoku⁽¹⁾, and Yutaka Tobita⁽²⁾

(1) Department of Physics, Faculty of Science,

Hokkaido University, Sapporo 060-0810, Japan and

(2) Department of Mathematics and Physics, Faculty of Science,

Hirosaki University, Hirosaki 036-8561, Japan

(Dated: September 25, 2021)

Abstract

This paper elucidates the anomalous decay of the muon ascribed to extended waves. Due to a large overlap of the parent and daughters, the transition amplitude and probability for the neutrinos are modified from the standard formula. A rigorous probability from the von Neumann's fundamental principle of the quantum mechanics at a large time interval T is, $P = T\Gamma + P^{(d)}$, where Γ is derived from the Fermi's golden rule, and $P^{(d)}$ is a correction term. A new term $P^{(d)}$ has origins in the overlapping waves, and influences the determinations of physical parameters. By including $P^{(d)}$, short-baseline neutrino experiments with LSND, KARMEN, and MiniBooNE become consistent each other and with the solar, long-baseline, and reactor experiments within the three neutrinos. Byproduct is that the absolute neutrino mass of the neutrinos can be measured.

arXiv:1405.0582v3 [hep-ph] 20 Jan 2017

I. INTRODUCTION

The muon decays

$$\begin{aligned}\mu^- &\rightarrow e^- + \bar{\nu}_e + \nu_\mu, \\ \mu^+ &\rightarrow e^+ + \nu_e + \bar{\nu}_\mu,\end{aligned}\tag{1}$$

are fundamental processes described by the interaction $\mathcal{L}_{int} = \frac{G_F}{\sqrt{2}} J_\rho(\mu, x) J^\rho(e, x)^\dagger$, where G_F is the Fermi coupling constant and $J_\rho(l, x)$ is the $V - A$ current of the charged lepton and the neutrino. The observed electron spectrum is in accord with the theoretical spectrum computed with the Fermi's golden rule precisely. It is expected that the neutrino spectrum would be consistent with the golden rule [1-3].

The decay is described by a many-body wavefunction, $|\Psi(t)\rangle$, which is a solution of the time-dependent Schrödinger equation with the Hamiltonian $H_0 + H_{int}$, where H_0 is the free part and $H_{int} = -\int d\vec{x} \mathcal{L}_{int}$. That is initially at a time $t = 0$ a one-muon state and develops a three-lepton component at later times. The state at a large t normally satisfies $\langle \Psi(t) | H_{int} | \Psi(t) \rangle = 0$, which represents free independent particles; we call this region a particle zone. A left figure in Fig.1 shows the waves in the particle zone. Using the transition probability $P(T)$ at $t = T$, which is defined with a square of the inner product of the states from the von Neumann's fundamental principle of the quantum mechanics (FQM) for normalized states, the average probability per unit of time $\Gamma = \frac{P(T) - P(T_0)}{T - T_0}$ between a large T and a small T_0 is determined by the Fermi's golden rule[1-3] for $P(T) \ll 1$. Now, states of $\langle \Psi(t) | H_{int} | \Psi(t) \rangle \neq 0$ shown in a right figure of Fig.1 also exist and give an independent contribution to the probability at T_0 . These represent interacting waves; we call this region a wave zone. Thus

$$P(T) = P(T_0) + \Gamma(T - T_0)\tag{2}$$

[4-7]. The neutrino in the muon decay is one of the cleanest systems that reveal intriguing properties of the wave zone, which is studied in the present paper.

Neutrino oscillation experiments disclosed the neutrino's masses and mixing angles. The values obtained with single-particle formula in long-distance region are consistent with each other [8], and the mass-squared differences of the neutrinos $\Delta m_{ij}^2 = m_{\nu_i}^2 - m_{\nu_j}^2$ are $(7.53 \pm 0.18) \times 10^{-5} \text{ eV}^2/c^4$ and $(2.44 \pm 0.06) \times 10^{-3} \text{ eV}^2/c^4$ (normal hierarchy) or $(2.51 \pm 0.06) \times 10^{-3} \text{ eV}^2/c^4$ (inverted). The formula gives negligible effect in short distance regions.

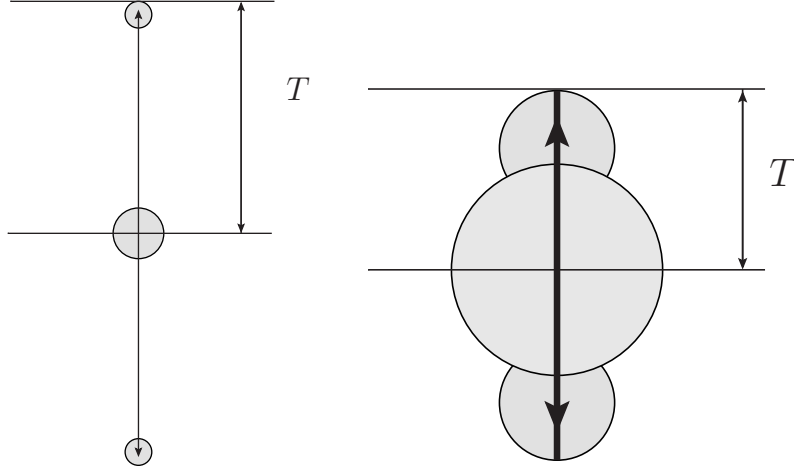


FIG. 1. Wavefunction of a two-body decay of a particle at rest in a configuration space at T in the particle zone (left) and in the wave zone (right). The shadow areas show the regions of the waves. In the particle zone, the states do not overlap and behave like particles. In the wave zone, they overlap and behave like interacting waves.

Nevertheless, signals have been found in experiments of LSND and MiniBooNE and fitted with much higher mass, but not in KARMEN. The discrepancy may be a signal beyond the standard model. Sterile neutrino is one of interesting possibilities and projects for its search are under ways. In these analyses, the neutrino in the particle zone were assumed. If neutrinos in the wave zone participate in the short-distance region, the oscillation formula will be modified. That could be related with the existing discrepancy, and deserves of intensive study.

In the transitions at the particle zone, the final waves separate quickly and the state is described by a stationary state of $\lim_{t \rightarrow \pm\infty} \langle \Psi(t) | H_{\text{int}} | \Psi(t) \rangle = 0$ [9–11]. They are described by a standard method of field theory, an S-matrix, $S[\infty]$ with an interaction Hamiltonian $e^{-\epsilon|t|} H_{\text{int}}$, in which the limit $\epsilon \rightarrow 0$ is taken at the end of the calculation. The interaction switches off adiabatically (ASI) and $\lim_{t \rightarrow \pm\infty} \langle \Psi_o(t) | e^{-\epsilon|t|} H_{\text{int}} | \Psi_i(t) \rangle = 0$ holds for arbitrary states $|\Psi_i(t)\rangle$ and $|\Psi_o(t)\rangle$. The probability proportional to the time interval T , ΓT , is derived. The neutrino spectrum is given by the single-particle formula.

The states of $\langle \Psi(t) | H_{\text{int}} | \Psi(t) \rangle \neq 0$ at large t are not described by ASI [12], and the transition probability from these states is not included in that of the golden rule or of $S[\infty]$. The probability computed with FQM [4–7] includes both, and is expressed in the two-body

decays as

$$P(T) = T\Gamma + P^{(d)}. \quad (3)$$

Here Γ agrees with that of the golden rule. From Eq.(2), $P^{(d)}$ given by $P^{(d)} = P(T_0) - \Gamma T_0$ shows a rapid transition of the extended waves at a small time. This is characterized by the angular velocity of the non-stationary neutrino at a position traveling with the speed of light $\omega = \frac{E_\nu(\vec{p}) - cp}{\hbar}$, where $\hbar = \frac{h}{2\pi}$ and h is the Planck constant, \vec{p} , $E_\nu(\vec{p}) = \sqrt{p^2 c^2 + m_\nu^2 c^4}$, m , and c are the momentum, energy, mass, and the speed of light, and $p = |\vec{p}|$. This ω corresponds to a length $L_c = \frac{c}{\omega}$ in the configuration space. L_c is twice of the product of the neutrino's Compton wavelength with the boost factor $\frac{E_\nu(\vec{p})}{m_\nu c^2}$, and much longer than the typical size of the stationary wave, de Broglie wavelength $\frac{\hbar}{p}$. Accordingly $P^{(d)}$ is large compared with ΓT_0 in the neutrino, but is small in the electron. The flavor-changing probability is modified from the single-particle formula.

The time-dependent Schrödinger equation which describes the muon decay is

$$\begin{aligned} i\hbar \frac{\partial}{\partial t} |\Psi(t)\rangle &= H |\Psi(t)\rangle = (H_0 + H_{\text{int}}) |\Psi(t)\rangle, \\ H_0 &= \int d\vec{x} \sum_{l=e,\mu} \left(\bar{l}(x) \left(\vec{\alpha} \cdot \vec{\nabla} + \beta m_l \right) l(x) + \bar{\nu}_l(x) \left(\vec{\alpha} \cdot \vec{\nabla} + \beta m_{\nu_l} \right) \nu_l(x) \right), \\ H_{\text{int}} &= \frac{G_F}{\sqrt{2}} \int d\vec{x} (\bar{\mu}(x) \gamma_\rho (1 - \gamma_5) \nu_\mu(x)) \gamma^\rho (\bar{e}(x) (1 - \gamma_5) \nu_e(x))^\dagger, \end{aligned} \quad (4)$$

for a case of no-mixing, and solved easily in the lowest order of G_F . For a muon of the lifetime τ_μ with average momentum \vec{p}_μ and the range in space covered by the wavefunction σ_μ in the initial state, a normalized solution $|\Psi(t), \vec{p}_\mu\rangle$ is

$$\begin{aligned} |\Psi(t), \vec{p}_\mu\rangle &= a_0(t) |\vec{p}_\mu; \sigma_\mu\rangle + \int d\vec{p}_e d\vec{p}_{\nu_e} d\vec{p}_{\nu_\mu} a_1(t, \vec{p}_e, \vec{p}_{\nu_e}, \vec{p}_{\nu_\mu}) |\vec{p}_e, \vec{p}_{\nu_e}, \vec{p}_{\nu_\mu}\rangle + O(G_F^2), \\ a_0(t) &= \left(\frac{1}{1 + \zeta(t)} \right)^{1/2} e^{-i \frac{E_\mu}{\hbar} t - \frac{t}{2\tau_\mu}}, \\ a_1(t, \vec{p}_e, \vec{p}_{\nu_e}, \vec{p}_{\nu_\mu}) &= \left(\frac{1}{1 + \zeta(t)} \right)^{1/2} e^{-i \frac{E_\mu}{\hbar} t} \frac{e^{-i \frac{\Delta E}{\hbar} t} - e^{-\frac{t}{2\tau_\mu}}}{\Delta E + i \frac{\hbar}{2\tau_\mu}} \langle \vec{p}_e, \vec{p}_{\nu_e}, \vec{p}_{\nu_\mu} | H_{\text{int}} | \vec{p}_\mu; \sigma_\mu \rangle, \end{aligned} \quad (5)$$

where $\Delta E = E_e + E_{\nu_e} + E_{\nu_\mu} - E_\mu$. The coefficients satisfy $a_0(0) = 1$, $a_1(0, \vec{p}_e, \vec{p}_{\nu_e}, \vec{p}_{\nu_\mu}) = 0$.

Using the matrix element given later,

$$(1 - e^{-\frac{t}{\tau_\mu}}) = \int_{\Delta E \approx 0} d\vec{p}_e d\vec{p}_{\nu_e} d\vec{p}_{\nu_\mu} \left| \frac{e^{-i\frac{\Delta E}{\hbar}t} - e^{-\frac{t}{2\tau_\mu}}}{\Delta E + i\frac{\hbar}{2\tau_\mu}} \langle \vec{p}_e, \vec{p}_{\nu_e}, \vec{p}_{\nu_\mu} | H_{\text{int}} | \vec{p}_\mu, \sigma_\mu \rangle \right|^2, \quad (6)$$

$$\zeta(t) = \int_{\Delta E \neq 0} d\vec{p}_e d\vec{p}_{\nu_e} d\vec{p}_{\nu_\mu} \left| \frac{e^{-i\frac{\Delta E}{\hbar}t} - e^{-\frac{t}{2\tau_\mu}}}{\Delta E + i\frac{\hbar}{2\tau_\mu}} \langle \vec{p}_e, \vec{p}_{\nu_e}, \vec{p}_{\nu_\mu} | H_{\text{int}} | \vec{p}_\mu, \sigma_\mu \rangle \right|^2, \quad (7)$$

where Eq.(7) is evaluated at a small $\frac{t}{\tau_\mu}$. τ_μ in Eq.(6) and $\zeta(t)$ in Eq.(7) signify the asymptotic behavior ascribed to the wavefunction in the particle zone and in the wave zone respectively. The right-hand side of Eq.(6) varies slowly with t , and the right-hand side of Eq.(7) increases rapidly at a small t and becomes constant at later times. Ignoring the rapid change,

$$\zeta(0) = 0, \quad \zeta(t) = \zeta < 1 (t > 0), \quad (8)$$

where ζ is a constant. Norm of $|\Psi(t), \vec{p}_\mu\rangle$ is the sum of the integrals over the momenta in $\Delta E \approx 0$ and $\Delta E \neq 0$,

$$\langle \Psi(t), \vec{p}_\mu | \Psi(t), \vec{p}_\mu \rangle = \frac{1}{1 + \zeta(t)} e^{-\frac{t}{\tau_\mu}} + \frac{1}{1 + \zeta(t)} (1 - e^{-\frac{t}{\tau_\mu}}) + \frac{\zeta(t)}{1 + \zeta(t)}, \quad (9)$$

where the first term in the right-hand side shows the norm of the muon, the second term shows that of the three leptons of $\Delta E \approx 0$, and the third one shows these of $\Delta E \neq 0$. A component of $\Delta E \approx 0$ results to $\Gamma = \frac{1}{\tau_\mu}$, and that of $\Delta E \neq 0$ results to $\zeta(t)$. The muon number decreases rapidly at a short time from $\zeta(t)$.

For $t \gg \tau_\mu$, $|a_0(t)| = 0$,

$$a_1(t) = \left(\frac{1}{1 + \zeta} \right)^{1/2} e^{-i\frac{E_\mu}{\hbar}t} \frac{e^{-i\frac{\Delta E}{\hbar}t}}{\Delta E + i\frac{\hbar}{2\tau_\mu}} \langle \vec{p}_e, \vec{p}_{\nu_e}, \vec{p}_{\nu_\mu} | H_{\text{int}} | \vec{p}_\mu, \sigma_\mu \rangle, \quad (10)$$

and

$$\langle \Psi(t), \vec{p}_\mu | \Psi(t), \vec{p}_\mu \rangle = \frac{1}{1 + \zeta} (1 + \zeta) = 1 \quad (11)$$

$$\begin{aligned} \delta E^2 &= \langle \Psi(t) | (i\hbar \frac{\partial}{\partial t} - E_\mu)^2 | \Psi(t) \rangle = \langle \Psi(t) | H_{\text{int}}^2 | \Psi(t) \rangle \\ &\geq \langle \Psi(t) | H_{\text{int}} | \Psi(t) \rangle \langle \Psi(t) | H_{\text{int}} | \Psi(t) \rangle = \zeta^2. \end{aligned} \quad (12)$$

$\zeta \neq 0$ leads $\delta E^2 \neq 0$. Thus $|\Psi(\infty)\rangle$ includes the states of the wave zone.

Substituting $\frac{t}{\tau_\mu} \ll 1$ to Eqs.(6) and (7), $\Gamma = \frac{1}{\tau_\mu}$ and $\zeta = P^{(d)}$ are expressed with the integrals in the right-hand sides. The former is equivalent to the Weisskopf-Wigner formula.

In Eq.(7), the upper limit is $\Delta E = \infty$. The states of $\Delta E \rightarrow \infty$ are characterized by Lorentz invariant spectrum, and lead a universal form to $P^{(d)}$. That is independent of the particle's spin and evaluated for a scalar neutrino first. Writing the interaction Hamiltonian in the form $\int d^3x J(x)\nu(x)$ with the neutrino $\nu(x)$ and a product of the parent $|P\rangle$ and other daughters $|D\rangle J(x)$, the amplitude that the neutrino of the momentum p_ν is detected is proportional to $\langle p_\nu, D | \int d^4x J(x)\nu(x) | P \rangle$. The probability is proportional to $\int d^4x d^4y \Delta_J(x-y)\Delta_\nu(x-y)$, where $\Delta_J(x-y) = \sum_D \langle P | J^\dagger(y) | D \rangle \langle D | J(x) | P \rangle$ is a source correlation function in the state of the parent $|P\rangle$ summed over $|D\rangle$, and $\Delta_\nu(x-y; p_\nu) = \langle p_\nu | \nu(x)\nu^\dagger(y) | p_\nu \rangle$ is the neutrino propagator. $\Delta_J(x-y)$ has a singular and long-range component and a short-range one. The former one comes from the states of $E_D \rightarrow \infty$ and is of the form $\Delta_J(x-y) \approx \delta((x-y)^2)$. Substituting this term,

$$\Delta_J(x-y)\Delta_\nu(x-y) = e^{i(E(\vec{p}_\nu) - c|\vec{p}_\nu| \cos \theta)(x^0 - y^0)/\hbar} \delta((x-y)^2), \quad (13)$$

where θ is the angle between \vec{p}_ν and $\vec{x} - \vec{y}$, and $E(\vec{p}_\nu) = \sqrt{\vec{p}_\nu^2 c^2 + m_\nu^2 c^4}$, which becomes at $\theta = 0$,

$$e^{i\omega(x^0 - y^0)} \delta((x-y)^2), \quad \omega = \frac{E(\vec{p}_\nu) - cp_\nu}{\hbar}. \quad (14)$$

The phase varies extremely slowly over the region $l \leq L_c$,

$$L_c = \frac{c}{\omega} = \frac{\hbar}{m_\nu c} \times \frac{2E(\vec{p}_\nu)}{m_\nu c^2}. \quad (15)$$

Thus in the extreme forward direction, $\theta = 0$, the wavefunction has an extremely long correlation, and the integrand Eq.(13) varies with $x^0 - y^0$ extremely slowly. The integral over x and y gets an extra contribution from large $|x^0 - y^0|$ region. A calculation showed that the probability $P^{(d)}$ is proportional to the range in space covered by the wavefunction σ_ν ,

$$P^{(d)} = \sigma_\nu \frac{\hbar E(\vec{p}_\nu)}{m_\nu^2 c^3} \times (\text{numerical factor}). \quad (16)$$

The length L_c and $\sqrt{\sigma_\nu}$ are much longer than the de Broglie wavelength. L_c is 2×10^2 meter for $E = 10$ MeV and $m_\nu c^2 = 10^{-1}$ eV, and its ratio over the de Broglie wavelength is roughly $(\frac{E}{m_\nu c^2})^2 = 10^{16}$. Accordingly, a frequency of the events determined by Eq.(16) is high. These are characteristic features of the interacting quantum waves in the wave zone. L_c is slightly smaller than the muon mean free length $c\tau_\mu$, and a delicate competition

between this diffraction and the decay gives a sensitive signal to the absolute neutrino mass. The long-range correlation similar to the EPR correlation [13, 14] appears and gives $P^{(d)}$.

Rigorous calculation is made later using the S-matrix $S[T]$ defined with the normalized functions of satisfying the boundary conditions at T based on FQM. The transition probability at T , $P(T)$, is computed without facing difficulty mentioned in [12]. $S[T]$ is formulated with the Møller operator, and wave packets localized in space, [4–7, 15]. LSZ formula

$$\begin{aligned}\lim_{t \rightarrow -T/2} \langle \alpha | \phi^f(t) | \beta \rangle &= \langle \alpha | \phi_{\text{in}}^f | \beta \rangle, \\ \lim_{t \rightarrow +T/2} \langle \alpha | \phi^f(t) | \beta \rangle &= \langle \alpha | \phi_{\text{out}}^f | \beta \rangle,\end{aligned}\tag{17}$$

are applied, where $\phi_{\text{in}}(x)$ and $\phi_{\text{out}}(x)$ satisfy the free wave equation, and $\phi^f(t)$, $\phi_{\text{in}}^f(t)$, and $\phi_{\text{out}}^f(t)$ are the expansion coefficients of $\phi(x)$, $\phi_{\text{in}}(x)$, and $\phi_{\text{out}}(x)$, with the normalized wave functions $f(x)$ of the form

$$\phi^f(t) = i \int d^3x f^*(\vec{x}, t) \overleftrightarrow{\partial}_0 \phi(\vec{x}, t).\tag{18}$$

It is noticed that a complete set of the normalized functions includes those that are specified by their centers in momentum space and in configuration space [15, 17].

$P^{(d)}$ has the origin in the long-range component of the wavefunction that depends on the initial and final states, and causes the rapid transition in short times. That shows unique properties. Because $P^{(d)}$ depends on the absolute mass, that of the neutrino is much larger than that of the electron, and the neutrino flavor change distinct from the standard oscillation may arise in the short-distance regions. $P^{(d)}$ may be directly connected with the inconsistency among previous experiments within three neutrino flavor.

The absolute neutrino masses are unknown now. One of existing methods is to study tritium beta decay, but the existing upper bound for the effective electron-neutrino mass-squared difference is approximately $2 \text{ eV}^2/c^4$ [18]. From cosmology, the bounds for a sum of masses are $0.44 \text{ eV}/c^2$ [19, 20] and $0.23 \text{ eV}/c^2$ [21]. They are important in structure formations in cosmology. They may be determined by precision experiments in short-distance regions.

The present paper analyzes the neutrino properties in the wave zone in detail including the mixing effects, and is organized in the following manner. In Sec. 2, the transition amplitudes and probability of the muon decay processes including the overlap effects are derived. In Sec. 3, its implications in the neutrino experiments are presented. Summary is given in Sec. 4.

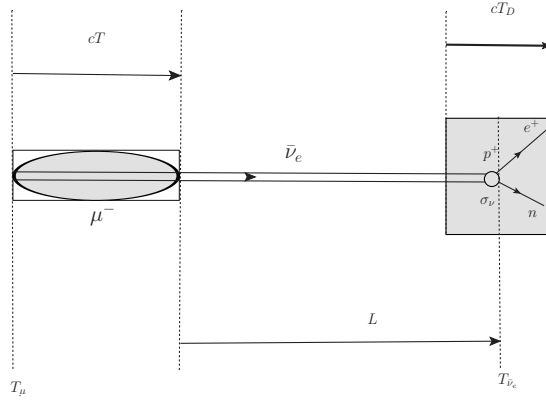


FIG. 2. The geometry of the μ^- decay at rest is shown. In real experiments, a detector with a length of cT_D is located away from the decay region. However, in Sec. 3 we study a case where a detector is located in front of the decay region, i.e., $L = 0$, for simplicity.

II. THE TRANSITION AMPLITUDE AND PROBABILITY

The normalized functions in configuration space in Eqs. (17) and (18) for outgoing states represent microscopic states that an outgoing state interacts with [4]. For the processes that the neutrinos are detected, they represent nucleus or atom bound in solid, which have almost uniform density and decrease smoothly toward the edge. They are approximated well with Gaussian wave packets [5]. For incoming states, they express the states in the beam. The muon in the beam has a finite range in space determined by the mean free path in medium. From here the natural unit is used in most places.

A. S-matrix at a finite-time interval $S[T]$

The $S[T]$ defined from the wavefunction at T satisfies the unitarity $S[T]S^\dagger[T] = 1$. Inserting the initial and final states of the muon decay,

$$\langle \mu | S[T] | \mu \rangle \langle \mu | S^\dagger[T] | \mu \rangle + \langle \mu | S[T] | e, \nu, \bar{\nu} \rangle \langle e, \nu, \bar{\nu} | S^\dagger[T] | \mu \rangle = 1. \quad (19)$$

Thus the survivable probability, $P(\mu^- \rightarrow \mu^-)$, is written with the decay probability, $P(\mu^- \rightarrow e^- + \nu_\mu + \bar{\nu}_e)$, as

$$P(\mu^- \rightarrow \mu^-) = 1 - P(\mu^- \rightarrow e^- + \nu_\mu + \bar{\nu}_e). \quad (20)$$

Later $P(\mu^- \rightarrow e^- + \nu_\mu + \bar{\nu}_e) = \Gamma T + P^{(d)}$ is computed. Depending on the magnitude of $P(\mu^- \rightarrow e^- + \nu_\mu + \bar{\nu}_e)$, that is written as

$$P(\mu^- \rightarrow \mu^-; T) = \begin{cases} 1 - (\Gamma T + P^{(d)}); & \text{small } P(\mu^- \rightarrow e^- + \nu_\mu + \bar{\nu}_e) \\ \frac{1}{1+P^{(d)}} e^{-\Gamma T}; & \text{other.} \end{cases} \quad (21)$$

The normalization of the muon is affected by the transition from Eq.(5).

1. $\mu \rightarrow e + \nu + \bar{\nu}$

In the case $m_\nu \approx 0.08$ eV, T_c in Eq. (15) satisfies $T_c \gg \tau_\mu$. The case $P \ll 1$ is studied first.

The detection of $\bar{\nu}_e$ through the inverse β process is shown in Fig. 2; cT is the muon decay region and D is the detector. The length between decay region and detector denoted L is set to zero in this section, but that is included in the latter section. We study first the single neutrino case, using the same notation for the particle and anti-particle: μ for μ^+ and μ^- , etc.

The decay amplitude of a muon of a wave packet denoted as $|\mu\rangle$ to a final state of plane waves for e and ν_μ and a wave packet for ν_e $|e, \nu_\mu, \nu_e\rangle$ [22]

$$|\mu\rangle = |\vec{p}_\mu, \vec{X}_\mu, T_\mu\rangle, \quad |e, \nu_\mu, \nu_e\rangle = |\vec{p}_e, \vec{p}_{\nu_\mu}, \vec{p}_{\nu_e}, \vec{X}_{\nu_e}, T_{\nu_e}\rangle \quad (22)$$

is

$$\mathcal{M} = \frac{G_F}{\sqrt{2}} 8 N_\mu^{-1} N_{\nu_e}^{-1} \varrho_\mu \varrho_e \varrho_{\nu_\mu} \varrho_{\nu_e} f I(\delta p), \quad \delta p = p_\mu - p_e - p_{\nu_\mu} - p_{\nu_e}, \quad (23)$$

$$I(\delta p) = \int_{T_\mu}^{T_{\nu_e}} dt \int d\vec{x} e^{-i\delta\phi(x)} w(x, X_\mu; \sigma_\mu) w(x, X_{\nu_e}; \sigma_{\nu_e}),$$

$$f = \bar{u}(\vec{p}_{\nu_\mu}) \gamma_\rho (1 - \gamma_5) u(\vec{p}_\mu) \bar{u}(\vec{p}_e) \gamma^\rho (1 - \gamma_5) u(\vec{p}_{\nu_e}),$$

$$\delta\phi(x) = \phi_\mu(x, \vec{p}_\mu) - \phi_e(x, \vec{p}_e) - \phi_{\nu_\mu}(x, \vec{p}_{\nu_\mu}) - \phi_{\nu_e}(x, \vec{p}_{\nu_e}),$$

$$N_\mu = \left(\frac{\sigma_\mu}{\pi}\right)^{\frac{3}{4}}, \quad N_{\nu_e} = \left(\frac{\sigma_{\nu_e}}{\pi}\right)^{\frac{3}{4}}, \quad \varrho_\alpha = \left(\frac{m_\alpha}{(2\pi)^3 E_\alpha}\right)^{\frac{1}{2}}, \quad (24)$$

$$\phi_\alpha(x, \vec{k}_\alpha) = E(\vec{k}_\alpha)(t - T_\alpha) - \vec{k}_\alpha \cdot (\vec{x} - \vec{X}_\alpha), \quad (\alpha = \mu, \nu_e), \quad (25)$$

$$\phi_\beta(x, \vec{p}_\beta) = E(\vec{p}_\beta)t - \vec{p}_\beta \cdot \vec{x}, \quad (\beta = e, \nu_\mu), \quad (26)$$

where the wavefunctions are

$$\begin{aligned} w(x, X_\mu; \sigma_\mu; \tau_\mu) &= e^{-\frac{1}{2\sigma_\mu}(\vec{x}-\vec{X}_\mu-\vec{v}_\mu(t-T_\mu))^2-\frac{t-T_\mu}{2\tau_\mu}}; \quad t-T_\mu \geq 0, \\ w(x, X_\nu; \sigma_\nu) &= e^{-\frac{1}{2\sigma_\nu}(\vec{x}-\vec{X}_\nu-\vec{v}_\nu(t-T_\nu))^2}. \end{aligned} \quad (27)$$

Now the spreading effect of the wave packet and a causality at large $|t-T_{\nu_e}|$ that the wave packet vanishes at $(t-T_{\nu_e})^2 - (\vec{x}-\vec{X}_{\nu_e})^2 \leq 0$ [15], are negligible, and are not expressed explicitly in most places.

B. Transition probability

The amplitude \mathcal{M} from Eq.(23), is substituted into the transition probability at T

$$P = \int d\vec{p}_e d\vec{p}_{\nu_\mu} d\vec{p}_{\nu_e} \frac{d\vec{X}_{\nu_e}}{(2\pi)^3} |\mathcal{M}|^2. \quad (28)$$

Averaging over the initial spins and summing over the final spins,

$$P = \left(\frac{\pi^2}{\sigma_\mu \sigma_{\nu_e}} \right)^{\frac{3}{2}} \frac{2^8 G_F^2}{E_\mu (2\pi)^3} \int \frac{d\vec{p}_e d\vec{p}_{\nu_\mu} d\vec{X}_{\nu_e} d\vec{p}_{\nu_e}}{E_e E_{\nu_\mu} E_{\nu_e} (2\pi)^{12}} (p_\mu \cdot p_{\nu_e})(p_e \cdot p_{\nu_\mu}) |I(\delta p)|^2. \quad (29)$$

1. $\mu \rightarrow e\nu\bar{\nu}$: transition probability: normal term

$|I(\delta p)|^2$ in Eq.(29) is expressed by an integrals over times. The integrand in small $t_1 - t_2$ region is characterized by the de Broglie wavelength, and much shorter than the cT . Hence the integral from this region determines ΓT from Appendix C, and is evaluated by the integral over the region $-\infty < t_1 - t_2 < \infty$. Then the effect of the muon's life-time is neglected, and T is replaced with ∞ . It follows

$$I^{\text{normal}}(\delta p) = \int_{-\infty}^{\infty} dt \int d\vec{x} e^{-i\delta\phi(x)} w(x, X_\mu; \sigma_\mu) w(x, X_{\nu_e}; \sigma_{\nu_e}). \quad (30)$$

and

$$\begin{aligned} |I^{\text{normal}}(\delta p)|^2 &= \left(\frac{2\pi(\sigma_\mu + \sigma_{\nu_e})}{(\vec{v}_\mu - \vec{v}_{\nu_e})^2} \right) \left(\frac{2\pi\sigma_\mu\sigma_{\nu_e}}{\sigma_\mu + \sigma_{\nu_e}} \right)^3 \exp \left[-\frac{\sigma_\mu + \sigma_{\nu_e}}{(\vec{v}_\mu - \vec{v}_{\nu_e})^2} (\delta p^0 - \vec{v}_0 \cdot \delta\vec{p})^2 \right] \\ &\times \exp \left[-\frac{\sigma_\mu\sigma_{\nu_e}}{\sigma_\mu + \sigma_{\nu_e}} \delta\vec{p}^2 - \frac{(\vec{X}_\mu - \vec{X}_{\nu_e})_T^2}{\sigma_\mu + \sigma_{\nu_e}} \right], \end{aligned} \quad (31)$$

where

$$\begin{aligned}\vec{v}_0 &= \frac{\sigma_\mu \vec{v}_{\nu_e} + \sigma_{\nu_e} \vec{v}_\mu}{\sigma_\mu + \sigma_{\nu_e}}, \quad \tilde{X}_\mu = \vec{X}_\mu - \vec{v}_\mu T_\mu, \quad \tilde{X}_{\nu_e} = \vec{X}_{\nu_e} - \vec{v}_{\nu_e} T_{\nu_e}, \\ (\tilde{X}_\mu - \tilde{X}_{\nu_e})_T &= \tilde{X}_\mu - \tilde{X}_{\nu_e} - \vec{n} \left(\vec{n} \cdot (\tilde{X}_\mu - \tilde{X}_{\nu_e}) \right), \quad \vec{n} = \frac{\vec{v}_\mu - \vec{v}_{\nu_e}}{|\vec{v}_\mu - \vec{v}_{\nu_e}|}.\end{aligned}\quad (32)$$

Integrating over \vec{X}_{ν_e} , the probability is written as

$$\begin{aligned}P^0 = \Gamma T &= T \frac{(\sigma_\mu \sigma_{\nu_e})^{\frac{3}{2}}}{|\vec{v}_\mu - \vec{v}_{\nu_e}| (\sigma_\mu + \sigma_{\nu_e})} \frac{2^4 G_F^2}{E_\mu (2\pi)^7} \int \frac{d\vec{p}_e d\vec{p}_{\nu_\mu} d\vec{p}_{\nu_e}}{E_e E_{\nu_\mu} E_{\nu_e}} (p_\mu \cdot p_{\nu_e}) (p_e \cdot p_{\nu_\mu}) \\ &\times \exp \left[-\frac{\sigma_\mu \sigma_{\nu_e}}{\sigma_\mu + \sigma_{\nu_e}} \delta \vec{p}^2 \right] \exp \left[-\frac{\sigma_\mu + \sigma_{\nu_e}}{(\vec{v}_\mu - \vec{v}_{\nu_e})^2} (\delta p^0 - \vec{v}_0 \cdot \delta \vec{p})^2 \right]\end{aligned}\quad (33)$$

[4], where $T = T_{\nu_e} - T_\mu$. The condition $T \ll \tau_\mu$ is satisfied in all experiments and assumed in this paper. Other region $T \approx \tau_\mu$ is given in Appendix A.

2. Spectral representation : finite-size corrections

The probability from the large $t_1 - t_2$ region in Eq.(29) is found from the expression

$$\begin{aligned}P &= \frac{2^5 G_F^2}{(\sigma_\mu \sigma_{\nu_e})^{\frac{3}{2}} E_\mu} \int \frac{d\vec{X}_{\nu_e} d\vec{p}_{\nu_e}}{E_{\nu_e} (2\pi)^6} \int d^4 x_1 d^4 x_2 \Delta_{e,\nu_\mu}(\delta x) e^{i p_{\nu_e} \cdot \delta x}, \\ &\times \prod_i w(x_i, X_\mu; \sigma_\mu; \tau_\mu) w(x_i, X_{\nu_e}; \sigma_{\nu_e}), \quad \delta x = x_1 - x_2,\end{aligned}\quad (34)$$

$$\Delta_{e,\nu_\mu}(\delta x) = \frac{1}{(2\pi)^6} \int \frac{d\vec{p}_e d\vec{p}_{\nu_\mu}}{E_e E_{\nu_\mu}} (p_\mu \cdot p_{\nu_e}) (p_e \cdot p_{\nu_\mu}) e^{i(p_e + p_{\nu_\mu} - p_\mu) \cdot \delta x}, \quad (35)$$

where $\Delta_{e,\nu_\mu}(\delta x)$ has a short-range component and a long-range one. The long-range component is extracted by writing it with an integral representation of Jost, Lehmann, and Dyson [23, 24], given in Appendix B,

$$\begin{aligned}\Delta_{e,\nu_\mu}(\delta x) &= \frac{p_\mu \cdot p_{\nu_e}}{2(2\pi)^2} \int_{m_e^2} dm^2 \rho(m^2) iD^+(\delta t, \delta \vec{x}; p_\mu, m), \\ \rho(m^2) &= m^2 - 2m_e^2 + \frac{m_e^4}{m^2},\end{aligned}\quad (36)$$

Using the momentum $Q^\rho = p_e^\rho + p_{\nu_\mu}^\rho - p_\mu^\rho$, $iD^+(\delta t, \delta \vec{x}; p_\mu, m)$ is expressed as

$$iD^+(\delta t, \delta \vec{x}; p_\mu, m) = \frac{1}{(2\pi)^3} \int d^4 Q \delta(Q^2 - m^2) \theta(Q^0) e^{iQ \cdot \delta x}, \quad (37)$$

and

$$m \leq m_\mu$$

$$iD^+(\delta t, \delta \vec{x}; p_\mu, m) = iD^+(\delta t, \delta \vec{x}; p_\mu, m)^{(1)} + iD^+(\delta t, \delta \vec{x})^{(2)} + iD^+(\delta t, \delta \vec{x}; p_\mu, m)^{(3)} \quad (38)$$

$$iD^+(\delta t, \delta \vec{x}; p_\mu, m)^{(1)} = \frac{1}{(2\pi)^3} \int_{Q^0=0}^{Q^0=p_\mu^0} \frac{d\vec{Q}}{2Q^0} e^{iQ \cdot \delta x} \quad (39)$$

$$iD^+(\delta t, \delta \vec{x})^{(2)} = \frac{i}{4\pi} \delta(\lambda) \epsilon(\delta t) \quad (40)$$

$$iD^+(\delta t, \delta \vec{x}; p_\mu, m)^{(3)} = \sum_{n=0}^{\infty} \frac{1}{n!} \left(\frac{\partial}{\partial \tilde{m}^2} \right)^n \left(-ip_\mu \cdot \frac{\partial}{\partial \delta x} \right)^n i\tilde{D}^+(\delta t, \delta \vec{x}; i\tilde{m}), \quad (41)$$

$$m_\mu < m$$

$$iD^+(\delta t, \delta \vec{x}; p_\mu, m) = 0, \quad (42)$$

where $\tilde{D}^+(\delta t, \delta \vec{x}; i\tilde{m})$ is the sum of the Bessel functions. The short-range components of these functions, which give the probability ΓT from Appendix A and C, were computed in the previous sub-section.

Now, $P^{(d)}$ is computed from $iD^+(\delta t, \delta \vec{x})^{(2)}$. This is derived from the states of $|\vec{Q}| \rightarrow \infty$, and has the long-range component, when the series in $iD^+(\delta t, \delta \vec{x}; p_\mu, m)^{(3)}$ converges. This condition is reduced to that of the momenta

$$2p_\mu \cdot p_{\nu_e} \leq m_\mu^2 - m^2, \quad (43)$$

which agrees also with a causality condition that the light-cone singularity is in the physical region. Due to the singular nature, the computation is made in the configuration space. That is similar to that of [5] and the details are given in Appendix C. For a muon of large σ_μ , $\frac{(\vec{v}_\mu - \vec{v}_{\nu_e})^2 T^2}{4\sigma_\mu} \ll 1$, the relevant term $\tilde{g}(\omega_{\nu_e}, T; \tau_\mu)$ in Eq.(C7) is written as $\tau_\mu(g(\omega_{\nu_e}, T; \tau_\mu) - g(\omega_{\nu_e}, \infty; \tau_\mu))$. Then $\tau_\mu \tilde{g}(\omega_{\nu_e}, T; \tau_\mu)$ gives the slowly varying component, whereas $g(\omega_{\nu_e}, \infty; \tau_\mu)$ is combined with other short-range terms. Substituting $\tilde{g}(\omega_{\nu_e}, T; \tau_\mu)$, it follows

$$P^{(d)} = \frac{2G_F^2}{E_\mu} \int \frac{d\vec{p}_{\nu_e} p_\mu \cdot p_{\nu_e}}{E_{\nu_e} (2\pi)^5} \int dm^2 \rho(m^2) [\sigma_{\nu_e} \mathcal{C} \tilde{g}(\omega_{\nu_e}, T; \tau_\mu)], \quad (44)$$

where the integral over the invariant mass

$$\int_{m_e^2}^{m_\mu^2 - 2p_\mu \cdot p_{\nu_e}} dm^2 \rho(m^2) \simeq \frac{(m_\mu^2 - 2p_\mu \cdot p_{\nu_e})^2}{2} \theta(m_\mu^2 - 2p_\mu \cdot p_{\nu_e}), \quad (45)$$

is substituted and \mathcal{C} is constant in p_{ν_e} and given in Appendix C for various cases.

Finally,

$$P = T\Gamma + P^{(d)}, \quad (46)$$

$$P^{(d)} = \mathcal{C} \frac{G_F^2}{E_\mu} \int \frac{d\vec{p}_{\nu_e}}{E_{\nu_e} (2\pi)^5} (p_\mu \cdot p_{\nu_e}) (m_\mu^2 - 2p_\mu \cdot p_{\nu_e})^2 \theta(m_\mu^2 - 2p_\mu \cdot p_{\nu_e}) \sigma_{\nu_e} \tilde{g}(\omega_{\nu_e}, T; \tau_\mu), \quad (47)$$

$$\Gamma = \int dE_{\nu_e} \frac{d\Gamma}{dE_{\nu_e}} = \int dE_{\nu_e} \frac{G_F^2}{2\pi^3} m_\mu^2 E_{\nu_e}^2 \left(1 - \frac{2E_{\nu_e}}{m_\mu}\right). \quad (48)$$

Γ is in agreement with the known rate. $P^{(d)}$ is expressed, after the tedious calculations, as

$$\begin{aligned} P^{(d)} &= \frac{G_F^2}{(2\pi)^5 E_\mu} \left(\tilde{J}_1(p_\mu) + \tilde{J}_2(p_\mu) \right) \quad (49) \\ &= \frac{G_F^2 \sigma_{\nu_e} \mathcal{C}}{(2\pi)^4 E_\mu |\vec{p}_\mu|} \left[\int_0^{E_{\min}} dE_{\nu_e} F_1(E_{\nu_e}) \tilde{g}(\omega_{\nu_e}, T; \tau_\mu) + \int_{E_{\min}}^{E_{\max}} dE_{\nu_e} F_2(E_{\nu_e}) \tilde{g}(\omega_{\nu_e}, T; \tau_\mu) \right] \\ F_1(E_{\nu_e}) &= E_{\nu_e}^2 \left[E_{\nu_e}^2 (p_\mu^{+4} - p_\mu^{-4}) - \frac{4}{3} E_{\nu_e} m_\mu^2 (p_\mu^{+3} - p_\mu^{-3}) + \frac{m_\mu^4}{2} (p_\mu^{+2} - p_\mu^{-2}) \right] \\ F_2(E_{\nu_e}) &= E_{\nu_e}^2 \left[E_{\nu_e}^2 \left\{ p_\mu^{-4} - \left(\frac{m_\mu^2}{2E_{\nu_e}} \right)^4 \right\} - \frac{4}{3} E_{\nu_e} m_\mu^2 \left\{ p_\mu^{-3} - \left(\frac{m_\mu^2}{2E_{\nu_e}} \right)^3 \right\} \right. \\ &\quad \left. + \frac{m_\mu^4}{2} \left\{ p_\mu^{-2} - \left(\frac{m_\mu^2}{2E_{\nu_e}} \right)^2 \right\} \right], p_\mu^\pm = E_\mu \pm |\vec{p}_\mu|. \end{aligned}$$

In the above equations, the integral over the angle θ between the momenta of μ and ν_e is made following the condition Eq. (43),

$$\cos \theta \leq \cos \theta_c = \frac{E_\mu}{|\vec{p}_\mu|} - \frac{m_\mu^2}{2|\vec{p}_\mu| |\vec{p}_{\nu_e}|}. \quad (50)$$

The $P^{(d)}$ depends on the neutrino absolute mass through $\tilde{g}(\omega_{\nu_e}, T; \tau_\mu)$.

C. Energy spectrum

1. Diffraction component

The energy spectrum of the diffraction component is given from Eq.(49) by

$$\begin{aligned} \frac{dP^{(d)}}{dE_{\nu_e}} &= \frac{G_F^2 \sigma_{\nu_e} \mathcal{C}}{(2\pi)^4 E_\mu |\vec{p}_\mu|} [F_1(E_{\nu_e}) \tilde{g}(\omega_{\nu_e}, T; \tau_\mu) \theta(E_{\min} - E_{\nu_e}) \\ &\quad + F_2(E_{\nu_e}) \tilde{g}(\omega_{\nu_e}, T; \tau_\mu) \theta(E_{\max} - E_{\nu_e}) \theta(E_{\nu_e} - E_{\min})]. \quad (51) \end{aligned}$$

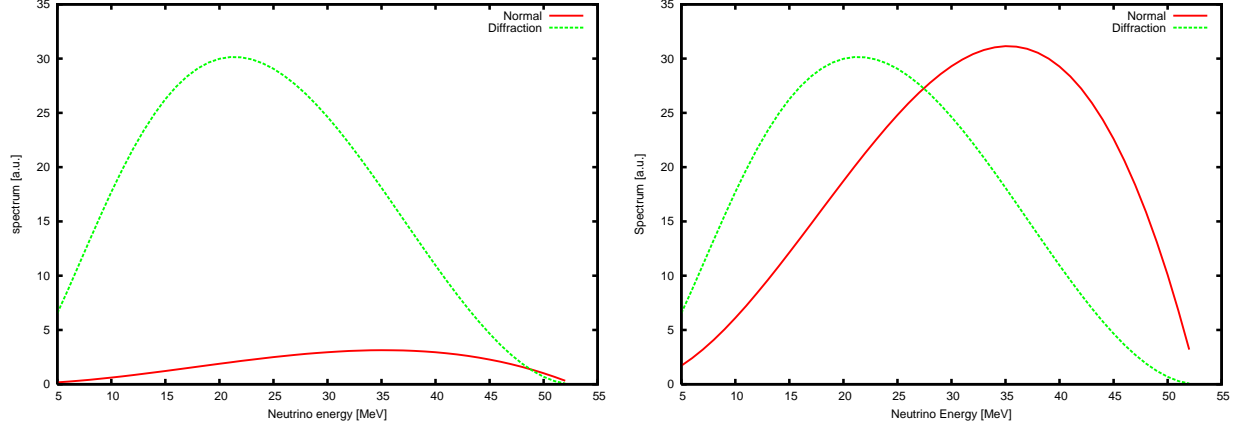


FIG. 3. (Color online) ν_e spectrum in μ DAR. The red curve shows the normal component given in Eq. (53), while the green curve shows the diffraction component given in Eq. (51). $m_{\nu_e} = 0.08$ eV, and $2\sigma_{\nu_e} = 12^{\frac{2}{3}}/m_\pi^2$ (^{12}C carbon target) were used in the numerical computation. Here, the detector is located at $L = 0$. The left figure corresponds to $cT = cT_D = 1$, the right figure to $cT = cT_D = 10$ m.

For the low-energy muon $|\vec{p}_\mu| \ll E_\mu \sim m_\mu$,

$$F_1(E_{\nu_e}) = |\vec{p}_\mu| \frac{m_\mu^7}{2} x^2 (1-x)^2, \quad F_2(E_{\nu_e}) = 0, \quad x = \frac{2E_{\nu_e}}{m_\mu}. \quad (52)$$

Eq. (51) and the spectrum at asymptotic region, Eq. (48) are given in Fig. 3 for a suitable value of σ_{ν_e} . At $cT = 1$ m, the diffraction term $P^{(d)}$ is considerably larger than the normal term in magnitude, and is about the same at $cT = 10$ m. Moreover, the peak shifts to lower energies by approximately 20 MeV. This arises from the fact that the dominant part of $P^{(d)}$ comes from the large momentum states and is derived from those satisfying the condition in Eq. (43). Currently, there are no precise data even for the electron in $x < 1/2$, and it would be interesting to confirm this component. The effect is reduced if the muon is a small wave packet. A low-energy negative muon in matter is trapped in an atom and forms a bound state with a small wave function; thus, the effect is reduced.

2. Normal component

From Eqs. (48), and (A2), the energy spectrum of the normal component of the muon decay at rest (μ DAR) in the asymptotic region is written as

$$\frac{dP^0}{dx} = \frac{G_F^2 m_\mu^5}{2(2\pi)^3} x^2 (1-x) \tau_\mu (1 - e^{-\frac{T_D}{\tau_\mu}}), \quad (53)$$

where T_D is the depth of the detector, which, for μ DAR, determines the time width. For the muon decay in flight (μ DIF), a decay region cT restricts the time width where μ exists. Those with suitable values, according to the experimental conditions, are used. The normal component of the transition rate or probability is independent of the size of the wave packets, from the completeness, but the energy spectrum depends on it and varies with the size. The spectrum for a plane wave given in Eq. (48) was confirmed in the upper energy region $x \geq 1/2$ of the electron spectrum.

D. Flavor mixing

1. Normal term

With three neutrino mass eigenstates of m_{ν_i} , $i = 1 - 3$, and $U_{\alpha,i}$, the flavor neutrino fields $\nu_l(x)$ in Eq. (4) are the linear combination of the fields of three $\nu_i(x)$ having mass m_i as

$$\nu_l(x) = \sum_i U_{l,i} \nu_i(x), \quad l = e, \mu, \tau, \quad (54)$$

where the best-fit values of the mixing angles given in Ref. [8]

$$\sin^2(\theta_{12}) = 0.304 \pm 0.014 \quad (55)$$

$$\sin^2(\theta_{23}) = 0.51 \pm 0.05 \text{ (normal hierarchy)}, \quad \sin^2(\theta_{23}) = 0.50 \pm 0.05 \text{ (inverted)},$$

$$\sin^2(\theta_{13}) = (2.19 \pm 0.12) \times 10^{-2}$$

are used, and a CP violation phase $\delta_{CP} = 0$ is assumed. The amplitudes for the anti-neutrino of flavor α to be detected in μ^+ decay ($\mu^+ \rightarrow \bar{\nu}_\mu + e^+ + \nu_e$) and for the neutrino of flavor α' in μ^+ decay ($\mu^+ \rightarrow \bar{\nu}_\mu + e^+ + \nu_e$) are

$$\begin{aligned} \mathcal{M}_{\alpha,\mu} &= \sum_i U_{\alpha,i} \mathcal{M}(\mu^+, i) U_{\mu,i}^*, \\ \mathcal{M}'_{\alpha',e} &= \sum_i U_{\alpha',i} \mathcal{M}'(\mu^+, i) U_{e,i}^*. \end{aligned} \quad (56)$$

The probability is the square of the amplitude,

$$P_{\alpha,\beta}^0 = |\mathcal{M}_{\alpha,\beta}|^2, \quad (57)$$

and is a function of $\sin^2 \frac{\Delta m_\nu^2 T}{4E_\nu}$ in the particle zone. For the two-flavor case, that is proportional to $4(\cos \theta \sin \theta)^2 \sin^2 \frac{\Delta m_\nu^2 T}{4E_\nu}$.

2. Diffraction term

The probability amplitude in the wave zone is described by the wavefunction of the correlation length L_c , and depends on the absolute neutrino mass and the flavor mixing matrix. The probability for a flavor change from α to β are expressed by a new universal function $\tilde{g}_{\alpha,\beta}(\omega_{\nu_\alpha}, T; \tau_\mu)$ as

$$P_{\alpha\beta}^{(d)} \propto \tilde{g}_{\alpha,\beta}(\omega_{\nu_\beta}, T; \tau_\mu) = \sum_{i,j} U_{\beta,i} U_{\alpha,i}^* U_{\beta,j}^* U_{\alpha,j} \tilde{g}(\omega_i, \omega_j, T; \tau_\mu). \quad (58)$$

These reflect the enhanced probability in short-distance regions, [28], accordingly the flavor change can be much larger than that of the normal term. They are studied in Appendix C. Some specific features are the following:

- (1) $\tilde{g}_{e,e}(\omega_{\nu_e})$ and $\tilde{g}_{\mu,e}(\omega_{\nu_e})$ are almost constant at $cT < 100$ m, and decrease uniformly at larger T . The values are sensitive to the absolute neutrino mass.
- (2) $\tilde{g}_{\mu,e}(\omega_{\nu_e})$ is significantly smaller than $\tilde{g}_{e,e}(\omega_{\nu_e})$, but not zero. That magnitude is proportional to $\tau_\mu(\omega_i + \omega_j)$ at a small $\tau\omega_i$ region. A new flavor changing effect arises in the short-distance region.

3. Flavor change in the short-distance region

The probability is the sum of those of Eqs.(57) and (58), and in the short-distance region,

$$P = C_0(4(\cos\theta \sin\theta)^2 (\frac{\Delta m_\nu^2 T}{4E_\nu})^2 + \tilde{g}_{\alpha,\beta}(\omega_{\nu_\beta}, T; \tau_\mu)), \quad (59)$$

for two flavor, where C_0 is a constant. The first term is proportional to the square of small quantity, but the second one is proportional to it. Thus the probability is determined by the second term.

The flavor change is determined by the diffraction in short-distance regions, but that is by the flavor oscillation in long-distance regions.

III. IMPLICATIONS TO NEUTRINO EXPERIMENTS

Been determined by the neutrino wavefunction, the standard formula depends on single-body properties such as the mass-squared difference $\Delta m_{\nu_{21}}^2 = m_{\nu_2}^2 - m_{\nu_1}^2$ and mixing angles. Now, $P^{(d)}$ is determined by the many-body wavefunction expressing the whole process of the

long distance correlation of the length, L_c , which is much longer than the typical detector size, and the final states from FQM. Accordingly, $P^{(d)}$ varies with the geometry and set up of the experiments. ΓT is equivalent in LSND and KARMEN, but $P^{(d)}$ is very different.

A. Boundary conditions for muon decays

In ground experiments, μ^+ (μ^-) is produced in π^+ (π^-) decay simultaneously with a ν_μ ($\bar{\nu}_\mu$), and decays to e^+ (e^-), $\bar{\nu}_\mu$ (ν_μ), and ν_e ($\bar{\nu}_e$). There are two typical types of experiments; one is the accelerator experiment that uses a neutrino beam from pion decay. In this case, both decays of high-energy π and μ are sources of neutrinos. The other is the experiment that observes the $\bar{\nu}_e$ or ν_μ appearance in μ^+ decay. In the latter, μ^+ is extracted and used as a source of neutrino, and π is not involved.

The nuclei wavefunctions in solid have ranges in space of the order of 10^{-15} m, while the electrons bound in the atoms have ranges in space of the order of 10^{-10} m. The neutrino and anti-neutrino interact differently with the matter [22]. For ν_e detected by the $^{12}\text{C} + \nu_e \rightarrow ^{12}\text{N}_{g.s.} + e^-$ process, that is the nucleus size

$$2\sigma_{\nu_e} = \frac{12^{\frac{2}{3}}}{m_\pi^2}, \quad (60)$$

of ^{12}C . For $\bar{\nu}_e$ detected by the inverse beta decay and delayed signal of neutron capture, the lightest nucleus H , i.e., the proton, and other nuclei are the targets. When $C_n H_{2n+2}$ is used for the scintillator, the size of the wave packet calculated from the ratio of the proton between C and H is

$$2\sigma_{\bar{\nu}_e} = \frac{3}{4} \frac{12^{\frac{2}{3}}}{m_\pi^2} + \frac{1}{4} \left(\frac{m_e a_\infty}{m_p + m_e} \right)^2, \quad (61)$$

where m_e and m_p are the masses of the electron and proton, respectively, and a_∞ is the used Bohr radius. For the detector, which consists of a mixture of several materials, the wave packet size becomes the value averaged over the abundance ratio of the materials.

The incoming muon is prepared in the apparatus. That propagates in matter or space with a mean free path

$$l_\mu = \frac{1}{n\sigma_{\text{cross}}}, \quad (62)$$

where n and σ_{cross} are the density of the scatterers and the cross section, respectively. They are determined by the transition rate and average lifetime of the velocity v

$$\Gamma = n\sigma_{\text{cross}}v = \frac{v}{l_{\mu}}, \quad \tau_{\text{int}} = \frac{1}{\Gamma}. \quad (63)$$

This is summarized in Ref. [8].

A pion is produced by a proton collision, hence, its range in space covered by the wave function is estimated from that of a proton. A proton mean free path of 1 GeV/ c was estimated as $l_{\text{proton}} = 50 - 100$ cm, and, at a lower momentum of 2 MeV/ c , $l_{\text{proton}} = 10$ cm. Analyzing the decay processes, we found that the range in space covered by the pion wave function at momentum 1 GeV/ c , or larger, is $\delta x_{\pi} \approx 40\text{-}100$ cm, and that by of the muon wave function of the momentum around 1 GeV/ c is $\delta x_{\mu} \approx 40\text{-}100$ cm. Thus, $\sigma_{\mu} = \pi(0.4 - 1.0)^2 \text{ m}^2$, and $\sigma_{\mu} = \infty$ is a good approximation.

μ^+ and μ^- decay in a symmetric manner in vacuum with the mean lifetime at rest $\tau_{\mu} = 2.2 \times 10^{-6}$ sec. However, due to the different charges they interact with atoms differently. For the stopped μ^+ , the wavefunctions in the periodic potential of a solid are extended waves with continuous energies. They are plane waves with phase shifts, and μ^+ at rest, $v = 0$, is described by a wavefunction covering a large range in space. The stopped μ^- can form bound states of localized wavefunctions and discrete energies. Thus, the wave packet for μ^- at rest has a short range. Consequently, μ^+ DAR is expressed by plane waves, while μ^- DAR is expressed by a wave packet of the small range. Both μ^{\pm} DIF are produced from decays of π^{\pm} and retain coherence of the same range of π^{\pm} . Therefore, it is a good approximation to treat μ^{\pm} DIF as plane waves [5]. Hereafter, we focus only on the μ^+ decay and study the above two types of experiments with $\sigma_{\mu} = \infty$.

B. ν_e and $\bar{\nu}_{\mu}$ in μ^+ decay

1. μ^+ decay at rest (μ^+ DAR)

In μ^+ DAR, the neutrino has the energy less than $m_{\mu}c^2$ and can produce the electron but not the muon. ν_e is detectable but $\bar{\nu}_{\mu}$ in charged current interactions is not. Nevertheless, the $\bar{\nu}_{\mu}$ spectrum is important to distinguish background events of the flavor oscillation

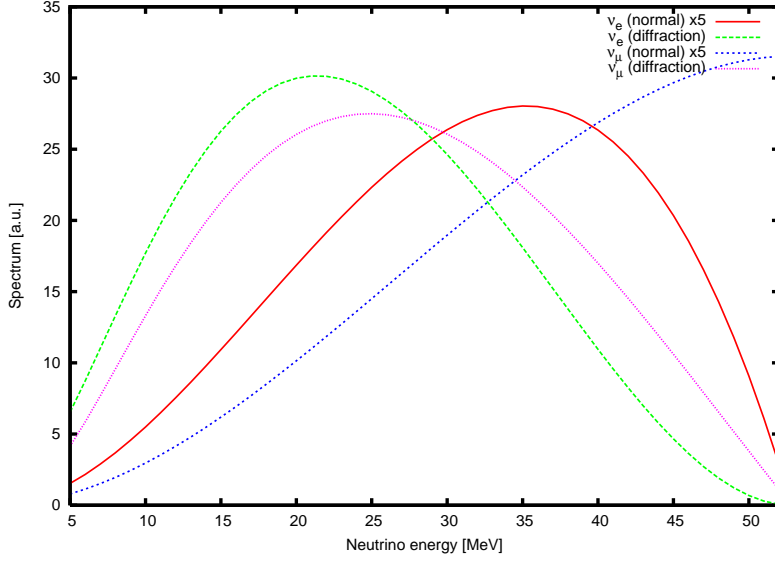


FIG. 4. (Color online) Spectra of normal and diffraction terms for ν_e and $\bar{\nu}_\mu$ in the μ^+ decay at rest. The spectra of the normal terms for ν_e (red) and $\bar{\nu}_\mu$ (blue) are different from those of ν_e (green) and $\bar{\nu}_\mu$ (magenta). These properties can be used to eliminate background events from μ^- decays, etc. $m_{\nu_h} = 0.08$ eV, $\sigma_\nu = 12^{\frac{2}{3}}/m_\pi^2$, $cT = cT_D = 1.0$ m, and inverted hierarchy are assumed in the numerical calculation.

phenomena. The energy spectra of the normal and diffraction terms for $\bar{\nu}_\mu$ are

$$\frac{dP^0}{dE_{\bar{\nu}_\mu}} = \frac{G_F^2 m_\mu^2}{12\pi^3} E_{\bar{\nu}_\mu}^2 \left(3 - 4 \frac{E_{\bar{\nu}_\mu}}{m_\mu} \right) \tau_\mu \left(1 - e^{-\frac{T_D}{\tau_\mu}} \right), \quad (64)$$

$$\frac{dP^{(d)}}{dE_{\bar{\nu}_\mu}} = \frac{G_F^2 m_\mu^2}{12\pi^3} \frac{E_{\bar{\nu}_\mu}^2 m_\mu^2 \sigma_{\bar{\nu}_\mu}}{4\pi} \left(1 - 2 \frac{E_{\bar{\nu}_\mu}}{m_\mu} \right) \left(5 - 6 \frac{E_{\bar{\nu}_\mu}}{m_\mu} \right) \tau_\mu \tilde{g}(\omega_{\bar{\nu}_\mu}, T; \tau_\mu), \quad (65)$$

and their ratio is

$$\begin{aligned} R(E_{\bar{\nu}_\mu}) &= \frac{dP^{(d)}}{dE_{\bar{\nu}_\mu}} / \frac{dP^0}{dE_{\bar{\nu}_\mu}} \\ &= \frac{m_\mu^2 \sigma_{\bar{\nu}_\mu}}{4\pi} \frac{\left(1 - 2 \frac{E_{\bar{\nu}_\mu}}{m_\mu} \right) \left(5 - 6 \frac{E_{\bar{\nu}_\mu}}{m_\mu} \right)}{3 - 4 \frac{E_{\bar{\nu}_\mu}}{m_\mu}} \frac{\tilde{g}(\omega_{\bar{\nu}_\mu}, T; \tau_\mu)}{1 - e^{-\frac{T_D}{\tau_\mu}}}. \end{aligned} \quad (66)$$

The energy spectra of the diffraction and normal terms for ν_e are given in Eqs. (51), and (53) and their ratio is

$$R(E_{\nu_e}) = \frac{\sigma_{\nu_e} m_\mu^2 \left(1 - \frac{2E_{\nu_e}}{m_\mu} \right)}{4\pi (1 - \exp[-T_D/\tau_\mu])} \tilde{g}_{e,e}(\omega_{\nu_e}, T; \tau_\mu), \quad (67)$$

Figure 4 shows the spectra obtained from Eqs. (51), (53), (64), and (65). The distinctive

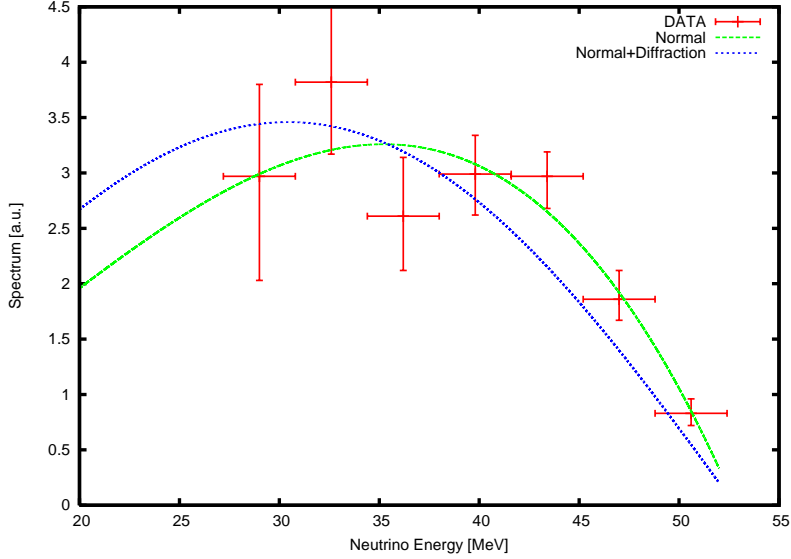


FIG. 5. (Color online) The spectra of normal and diffraction terms for ν_e are compared with KARMEN data. The green curve indicates the ν_e spectrum with normal term, while the blue curve indicates the sum of normal and diffraction terms; the crosses indicate the KARMEN experiment. Suitable parameters are chosen and relative magnitudes are shown.

spectra with peaks in the lower energy regions and the unique property that the magnitude varies with T and σ_{ν_e} , facilitate their differentiation from background events.

According to Fig.4, the ratios in Eqs. (66) and (67) are approximately equal to 5 at $cT = 1$ m with $m_{\nu_h} = 0.08$ eV of the inverted hierarchy. This value is quite large compared with that of the π decay [28]: if it is possible to identify ν_e from μ^+ DAR and collect sufficient statistics, it may be feasible to observe the excess of the ν_e flux and measure the absolute neutrino mass. The spectrum from KARMEN experiment is compared with the normal and diffraction terms in Fig. 5. The statistics are insufficient, and both theories are not in-consistent with the experimental results.

2. μ^+ decay in flight (μ^+ DIF)

The energy spectra of ν_e in μ^+ DIF are

$$\frac{d^2 P_{\nu_e}^0}{dE_{\nu_e} d \cos \theta} = \frac{2G_F^2 E_{\nu_e}^2}{(2\pi)^3 E_\mu} (E_\mu - p_\mu \cos \theta) (m_\mu^2 - 2p_\mu \cdot p_{\nu_e}) \gamma \tau_\mu \left(1 - \exp \left[-\frac{T}{\gamma \tau_\mu} \right] \right), \quad (68)$$

$$\frac{d^2 P_{\nu_e}^{(d)}}{dE_{\nu_e} d \cos \theta} = \frac{G_F^2 E_{\nu_e}^2}{(2\pi)^4 E_\mu} (E_\mu - p_\mu \cos \theta) (m_\mu^2 - 2p_\mu \cdot p_{\nu_e})^2 \sigma_{\nu_e} \gamma \tau_\mu \tilde{g}_{e,e}(\omega_{\nu_e}, T; \gamma \tau_\mu), \quad (69)$$

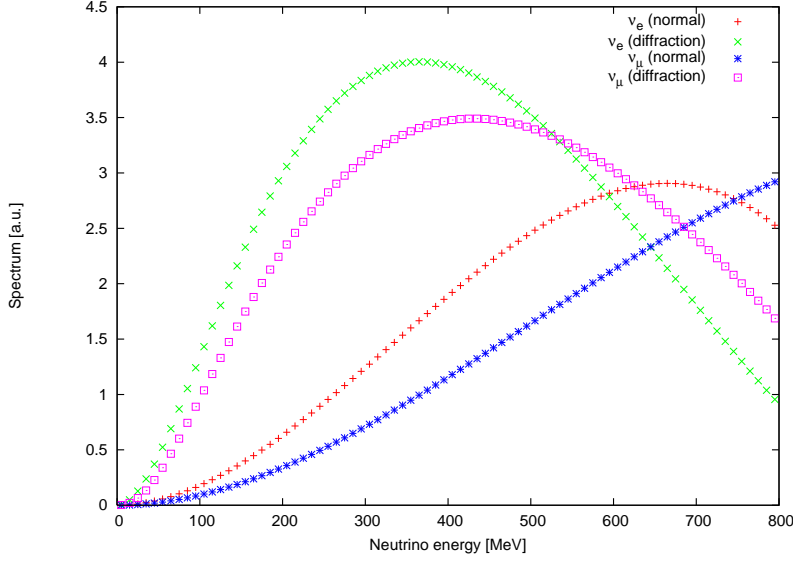


FIG. 6. (Color online) Spectra of the normal and diffraction terms for ν_e and $\bar{\nu}_\mu$ in μ^+ DIF. The spectra of the normal terms for ν_e (red) and $\bar{\nu}_\mu$ (blue) are different from those of ν_e (green) and $\bar{\nu}_\mu$ (magenta). These properties can be used to eliminate background events from μ^- decays, etc. $m_{\nu_h} = 0.08$ eV, $\sigma_\nu = 12^{\frac{2}{3}}/m_\pi^2$, $cT = 200$ m, $\cos\theta = 1$, and $E_\mu = 1$ GeV were used, and inverted hierarchy was assumed in the numerical calculation.

where θ is an angle between \vec{p}_μ and $\vec{p}_{\bar{\nu}_\mu}$; and $\gamma = E_\mu/m_\mu$; The energy spectra of $\bar{\nu}_\mu$ are

$$\frac{d^2 P_{\bar{\nu}_\mu}^0}{dE_{\bar{\nu}_\mu} d\cos\theta} = \frac{G_F^2 E_{\bar{\nu}_\mu}^2}{24\pi^3 E_\mu} [(E_\mu - p_\mu \cos\theta)(3m_\mu^2 - 4E_{\bar{\nu}_\mu}(E_\mu - p_\mu \cos\theta))] \times \gamma\tau_\mu \left(1 - \exp\left[-\frac{T}{\gamma\tau_\mu}\right]\right), \quad (70)$$

$$\frac{d^2 P_{\bar{\nu}_\mu}^{(d)}}{dE_{\bar{\nu}_\mu} d\cos\theta} = \frac{G_F^2}{24\pi^3 E_\mu} \frac{E_{\bar{\nu}_\mu}^2}{4\pi} (E_\mu - p_\mu \cos\theta)(m_\mu^2 - 2E_{\bar{\nu}_\mu}(E_\mu - p_\mu \cos\theta)) \times (5m_\mu^2 - 6E_{\bar{\nu}_\mu}(E_\mu - p_\mu \cos\theta))\gamma\tau_\mu\sigma_{\bar{\nu}_\mu}\tilde{g}_{\mu,\mu}(\omega_{\bar{\nu}_\mu}, T; \gamma\tau_\mu). \quad (71)$$

The ratios between the normal and diffraction terms for ν_e and $\bar{\nu}_\mu$ are

$$R(E_{\nu_e}, \cos\theta) = \frac{\sigma_{\nu_e}}{4\pi} (m_\mu^2 - 2E_{\nu_e}(E_\mu - p_\mu \cos\theta)) \frac{\tilde{g}_{e,e}(\omega_{\nu_e}, T; \gamma\tau_\mu)}{1 - \exp[-T/\gamma\tau_\mu]}, \quad (72)$$

$$R(E_{\bar{\nu}_\mu}, \cos\theta) = \frac{\sigma_{\bar{\nu}_\mu}}{4\pi} \frac{(m_\mu^2 - 2E_{\bar{\nu}_\mu}(E_\mu - p_\mu \cos\theta))(5m_\mu^2 - 6E_{\bar{\nu}_\mu}(E_\mu - p_\mu \cos\theta))}{3m_\mu^2 - 4E_{\bar{\nu}_\mu}(E_\mu - p_\mu \cos\theta)} \frac{\tilde{g}_{\mu,\mu}(\omega_{\bar{\nu}_\mu}, T, \gamma\tau_\mu)}{(1 - \exp[-T/\gamma\tau_\mu])}. \quad (73)$$

The spectra obtained from Eqs. (68)–(71) are shown in Fig. 6. They indicate that $R(E_{\bar{\nu}_\mu})$ and $R(E_{\nu_e})$ for on-axis $\bar{\nu}_\mu$ and ν_e are approximately equal to one with $E_\mu = 1$ GeV,

$m_{\nu_h} = 0.08$ eV with inverted hierarchy, and σ_ν of nuclear size at $cT = 200$ m. As this effect is clear and unique, this may be observed in high-energy neutrino experiments, even at small neutrino flux. In the next section, these findings will be compared with the existing experimental results.

3. Excess of electron neutrino in accelerator experiments

The accelerator experiments use a neutrino beam produced by π decays. In π^+ decay, ν_e is produced by the following processes

$$\pi^+ \rightarrow \mu^+ + \nu_\mu, \quad (74)$$

$$\mu^+ \rightarrow e^+ + \bar{\nu}_\mu + \underline{\nu_e}, \quad (75)$$

$$\rightarrow e^+ + \underline{\nu_e}, \quad (76)$$

and has two sources. $P^{(d)}$ in the ν_e mode is not suppressed, because the helicity-suppression works only to ΓT . That has been compared with the existing data of MiniBooNE in [28, 31], and all corrections, including those from the muon decay, are compared here. Lifetime of μ^+ and π^+ are also included.

We compare the result $\Gamma T + P^{(d)}$ with the MiniBooNE. $P^{(d)}$ of ν_e in Eq. (76), from Ref. [28], and that of ν_e from μ^+ of Eq. (75), is given in Fig. 7. Figure 7 indicates that our numerical results for the ratio between normal and diffraction modes are in agreement with the data. Furthermore, this shows that $P^{(d)}$ in the μ^+ decay dominates in ν_e events of MiniBooNE experiments, and is sensitive to the absolute mass value of the neutrino and the mass hierarchy. Our results are consistent within experimental uncertainties and Monte Carlo simulations with absolute neutrino mass values of $m_{\nu_h} = 0.07 - 0.08$ eV. This is consistent with our previous results [28]. Figure 8 shows the energy dependence of the ratio $P_{\nu_e}^{(d)}/P_{\nu_e}^{(0)}$ of our theory in a MicroBooNE experiment [32]. In this experiment, the neutrino beam is the same as that in the MiniBooNE experiment. The MicroBooNE detector is smaller than that of MiniBooNE, but the target nucleus is ^{40}Ar , whose range in space covered is substantially larger than that of ^{12}C , and the finite-size correction becomes also large. By using two different lengths of the decay region and sufficient statistics, not only the mass hierarchy, but also the absolute neutrino mass can be determined.

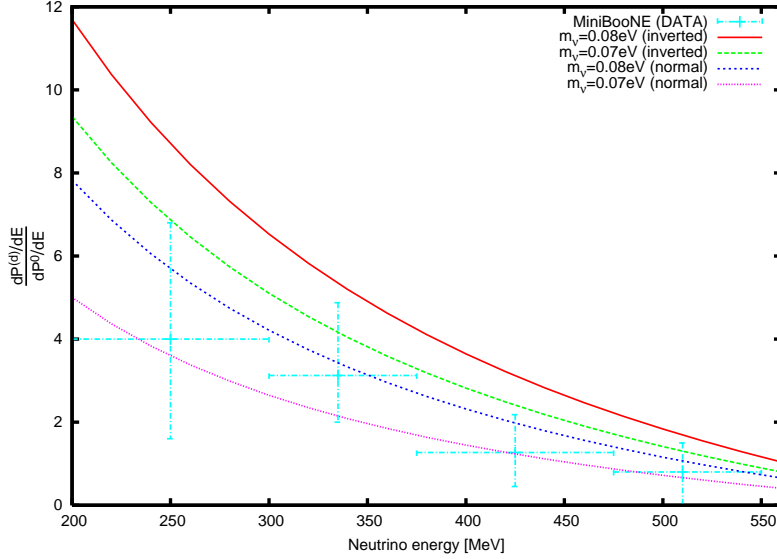


FIG. 7. (Color online) $P_{\nu_e}^{(d)}/P_{\nu_e}^{(0)}(\mu)$ is compared with the MiniBooNE data (light-blue) including statistic and systematic errors [31]. In the numerical calculation, $m_{\nu_h} = 0.07$ eV (green: inverted, magenta: normal), $m_{\nu_h} = 0.08$ eV (red: inverted, blue: normal), $E_\mu = 670$ MeV, and $E_\pi = 1.15$ GeV are used.

C. Neutrino flavor changes through diffraction

$P^{(d)}$ in the system of flavor mixing shows a unique behavior distinct from the standard formula. In μ^+ DAR, Eq.(2), $\bar{\nu}_e$ produced by the flavour mixing is sizable numbers and is detected at detectors with $L \sim 10 - 100$ m, if a range in space covered by the wavefunctions is large even with a small Δm^2 . In μ^+ DIF, both ν_μ and $\bar{\nu}_\mu$ have excesses.

1. LSND and KARMEN (μ^+ DAR)

Detector geometries of μ^+ DAR in LSND [26] and KARMEN [33] are similar but not identical. That of the μ^+ DAR experiment is shown in Fig. 9. μ^+ at rest decays in matter and $\bar{\nu}_e$, which is from $P^{(d)}$, propagates and is detected at downstream through inverse beta process with the delayed coincidence. T is a time interval in which μ^+ and its decay products co-exist and overlap. L is the spatial length between the decay region and the detector, and Δt is the time interval between the photon signals of the positron and neutron captures, used for event selection in KARMEN experiments. Δt is not taken into account in LSND. In the

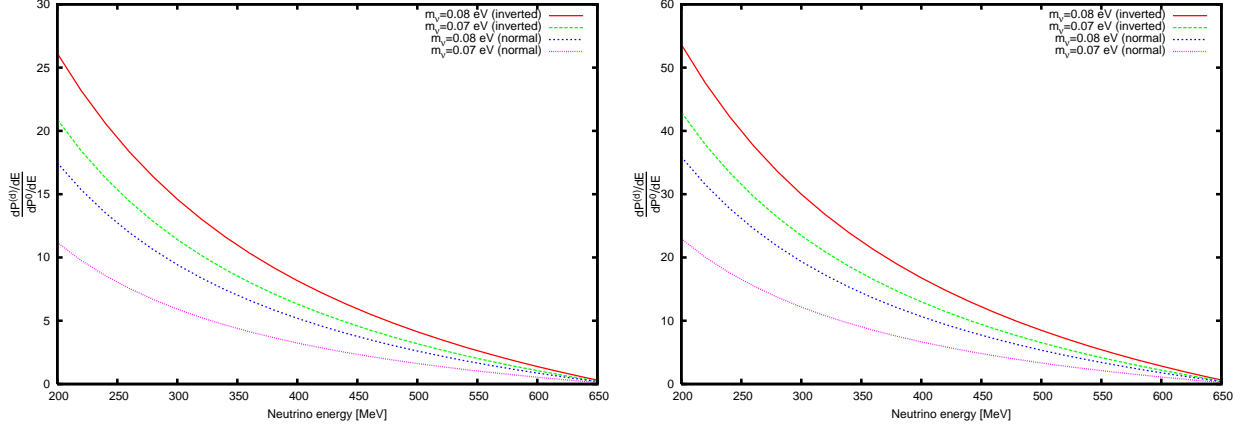


FIG. 8. (Color online) Energy dependences of the ratio $P_{\nu_e}^{(d)}/P_{\nu_e}^0$ from our theory for MicroBooNE [32] setup. The left figure corresponds to $cT = 50$ m; the right figure to $cT = 25$ m. In the numerical calculation, $m_{\nu_h} = 0.07$ eV (green: inverted, magenta: normal), $m_{\nu_h} = 0.08$ eV (red: inverted, green: normal), $E_\mu = 670$ MeV, and $E_\pi = 1.15$ GeV were used. The target nucleus is ^{40}Ar .

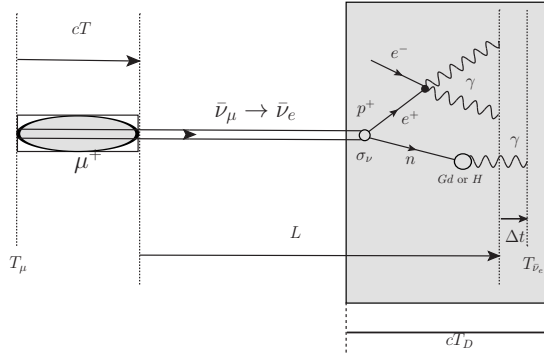


FIG. 9. Space-time geometry of the detection of $\bar{\nu}_e$ through inverse beta process with the delayed coincidence in μ^+ DAR. T is the time width where μ^+ and its decay products can overlap. L is the length between the decay region and the detector used in the flavor oscillation formula. Δt is the time difference between the photon signals of the positron and neutron captures, used for event selection in KARMEN experiments.

anti-neutrino events, photons from the positron annihilation arrive to the detector first, and the photon from the neutron capture arrive later, for the neutrino in the particle zone. The neutrino has the short-correlation length, and the delay time is sharply distributed in the order few μ seconds. Now, the neutrino in the wave zone represents the rapid transition in the short-time interval, and spreads over wide kinetic-energy region. That has the correlation

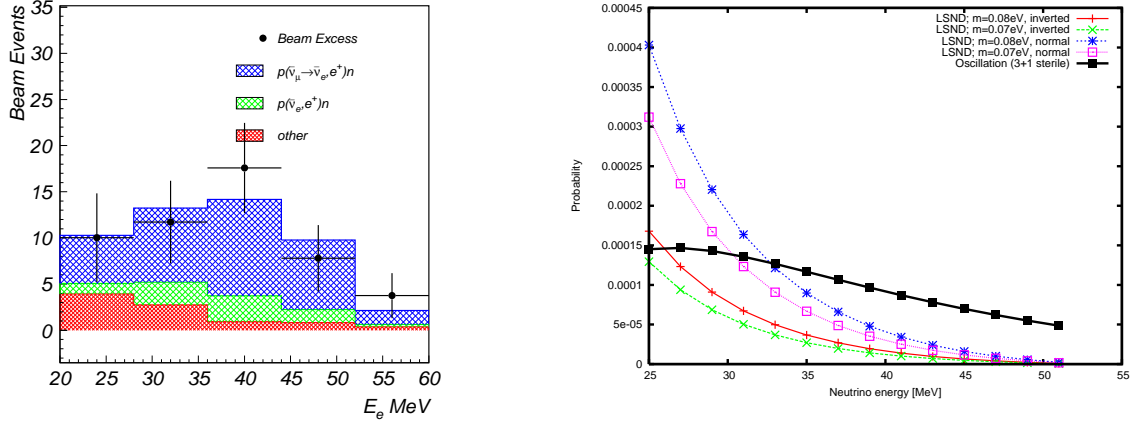


FIG. 10. (Color online) Spectra of LSND [27] (top) is compared with those of the neutrino oscillation due to the sterile neutrino (black line) and to the diffraction terms (colored line) in the bottom. $T_\mu = 0$, $cT = 0.8$ m ($T \sim 2.5$ ns), $cT_D = 8.3$ m, $L = 29.8$ m, $\sigma_{\bar{\nu}_e}^{\text{LSND}}$ of $C_{2n}H_{2n+2}$, $\Delta m_{LSND}^2 = 1.2$ eV², and $\sin^2 2\theta_{LSND} = 0.003$ are used. The red and green curves show the inverted hierarchy of $m_{\nu_h} = 0.08$ eV and $m_{\nu_h} = 0.07$ eV; the blue and magenta curves show the normal hierarchy of $m_{\nu_h} = 0.08$ eV and $m_{\nu_h} = 0.07$ eV.

length L_c . The neutron has the same properties, and interacts strongly with nucleus due to strong interaction through $P^{(d)}$ without thermalize, and emits a photon in the short-time interval. Hence photons from two processes arrive to detector almost simultaneously. By the timing cut, the neutrino events by $P^{(d)}$ may be rejected.

The diffraction term has an energy spectrum

$$\frac{dP^{(d)}}{dE_{\bar{\nu}_e}} = \frac{G_F^2 m_\mu^2 \tau_\mu}{12\pi^3} E_{\bar{\nu}_e}^2 \frac{m_\mu^2 \sigma_{\bar{\nu}_e}}{8\pi} \left(1 - 2\frac{E_{\bar{\nu}_e}}{m_\mu}\right) \left(5 - 6\frac{E_{\bar{\nu}_e}}{m_\mu}\right) \tilde{g}_{\mu,e}(\omega_{\bar{\nu}_e}, T; \tau_\mu), \quad (77)$$

where $\tilde{g}_{\mu,e}$ is given in Appendix C. The spectrum for three flavor are given in Fig.10, and are compared with the spectrum from LSND experiment. The event selection using the Δt is not made, but LSND adopted the likelihood ratio instead of Δt . The experimental parameters are summarized in Table I. The flavor change through $P^{(d)}$ in the experimental condition of KARMEN, $5\mu\text{s} < \Delta t < 300\mu\text{s}$ is given in Fig.11, and almost disappears. Thus a small difference in Δt causes an essential difference. This is understandable from the fact that the photons from two processes arrive to the detector almost simultaneously. The flavor change through $P^{(d)}$ in the experimental conditions of LSND and that of KARMEN are compared further.

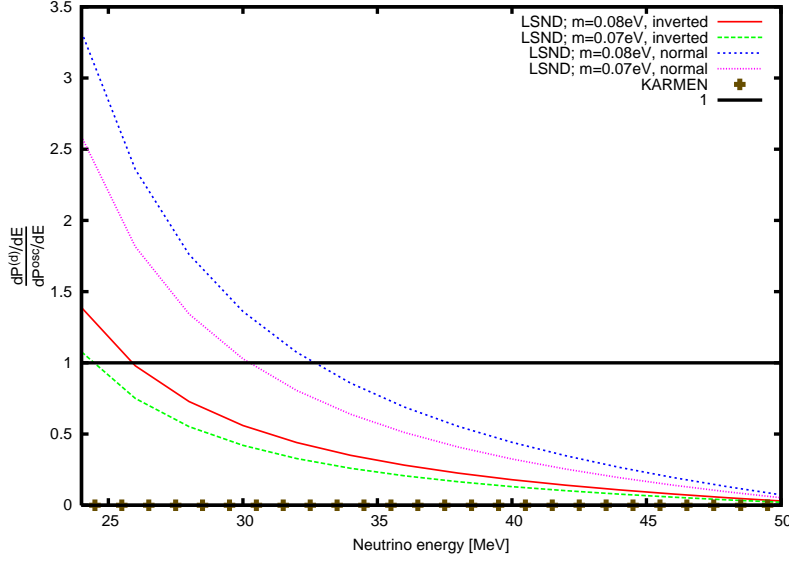


FIG. 11. (Color online) The ratios $\frac{dP^{(d)}/dE}{dP^{osc}/dE}$ are shown. For LSND, $T_\mu = 0$, $cT = 0.8$ m ($T \sim 2.5$ ns), $cT_D = 8.3$ m, $L = 29.8$ m, $\sigma_{\bar{\nu}_e}^{LSND}$ of $C_{2n}H_{2n+2}$, $\Delta m_{LSND}^2 = 1.2$ eV², and $\sin^2 2\theta_{LSND} = 0.003$ are used. The red curve shows the inverted hierarchy of $m_{\nu_h} = 0.08$ eV; the green curve shows the inverted hierarchy of $m_{\nu_h} = 0.07$ eV; the blue curve shows the normal hierarchy of $m_{\nu_h} = 0.08$ eV; the magenta curve shows the normal of $m_{\nu_h} = 0.07$ eV. For KARMEN, $T_\mu = 0.3$ μ s, $\Delta t = 5$ μ s, $cT = 0.3$ m ($T \sim 1.0$ ns), $cT_D = 3.5$ m, $m_{\nu_h} = 0.08$ eV of inverted hierarchy, $L = 17.7$ m, angle between proton beam and detector $\theta = 100^\circ$, $\sigma_{\bar{\nu}_e}^{KARMEN}$, $\Delta m_{LSND}^2 = 1.2$ eV² and $\sin^2 2\theta_{LSND} = 0.003$ are used. A geometry for μ^+ DAR is shown in Fig. 9 and a relation between T and θ is given in Appendix C 4.

For a comparison of the flavor change through $P^{(d)}$ in the experimental conditions of LSND and of KARMEN, the standard oscillation formula of two neutrino of the mass-squared difference Δm^2 derived from Γ

$$\frac{dP^{osc}}{dE_{\bar{\nu}_e}} = \frac{G_F^2 m_\mu^2 \tau_\mu}{12\pi^3} E_{\bar{\nu}_e}^2 \left(3 - 4 \frac{E_{\bar{\nu}_e}}{m_\mu} \right) \left(e^{-\frac{T_\mu}{\tau_\mu}} - e^{-\frac{(T_\mu + T_D)}{\tau_\mu}} \right) \sin^2 2\theta \sin \left(1.27 \frac{\Delta m^2}{E_\nu} L \right), \quad (78)$$

which is less sensitive to the experimental conditions, is used as a reference. Their ratios $\frac{dP^{(d)}/dE}{dP^{osc}/dE}$, following the parameters shown in Table I are computed. As Fig. 9 shows, the detector is located away from the muon decay area, and the parent and daughters overlap in a finite range covered by the wave functions $T = T_{\bar{\nu}_e} - T_\mu - L/c$. There are two cases:

1. No cut is required on the time difference Δt between the photons from positron and

	LSND	KARMEN
Size of beam stop (D×W×H)	1 m×0.2 m×0.2 m	0.5 m× 0.25 m×0.25 m
L	29.8 m	17.7 m
Δt	No	$5 \mu\text{s} < \Delta t < 300 \mu\text{s}$
Scintillator	CH_2	$C_nH_{2n+2}(75\%) + C_9H_{12}(25\%)$
$E_{\bar{\nu}_e}$	36(20)–60 MeV	16–50 MeV
Primary positron time window	No, $T_\mu = 0$	$0.6 \mu\text{s} < T_\mu < 10 \mu\text{s}$
T_D , Depth of detector	8.3 m	3.5 m
Detector angle	10°	100°
$\bar{\nu}_e$ event excess	$87.9 \pm 22.4 \pm 6.0$	No excess
Best fit Δm^2 and $\sin^2 \theta$	$\Delta m^2 = 1.2 \text{ eV}^2$, $\sin^2 \theta = 0.003$	None

TABLE I. Parameters and results of LSND and KARMEN.

those from neutron:

In this case, the overlapping region is determined by the interval between the initial and final instant of times, and the range covered by the beam stop, and is wide. Hence, the diffraction term is included into the event of $\bar{\nu}_e$.

2. Cut on Δt is made.

In this case, the overlapping region is reduced by Δt as $T = T_{\bar{\nu}_e} - T_\mu - L/c - \Delta t$. Only for $T > 0$, the waves overlap, and $P^{(d)} \neq 0$. In other case, the waves do not overlap and $P^{(d)} = 0$.

LSND did not use the cut and included all the events. Consequently, the diffraction was included. Now, KARMEN selected the events of satisfying $\Delta t > 5 \mu\text{s}$, and excluded the events of $\Delta t < 5 \mu\text{s}$, which corresponds to the length $\Delta L = 1.5 \times 10^3$ meters from our estimation. This condition does not affects the events due to Γ , because the correlation length is much shorter.

The theoretical value of $P^{(d)}$ for LSND and KARMEN are shown in Fig. 11. $P^{(d)}$ in LSND configuration is large, while that for KARMEN configuration vanishes. If $\bar{\nu}_e$ excess is verified from events of $\Delta t < 5 \mu\text{s}$ in the KARMEN experiment, that proves the present theory. A precise dependence on Δt of the ratio is given in Fig. 12. The magnitude of $P^{(d)}$ is approximately ten times larger than that of LSND because L of KARMEN is shorter than

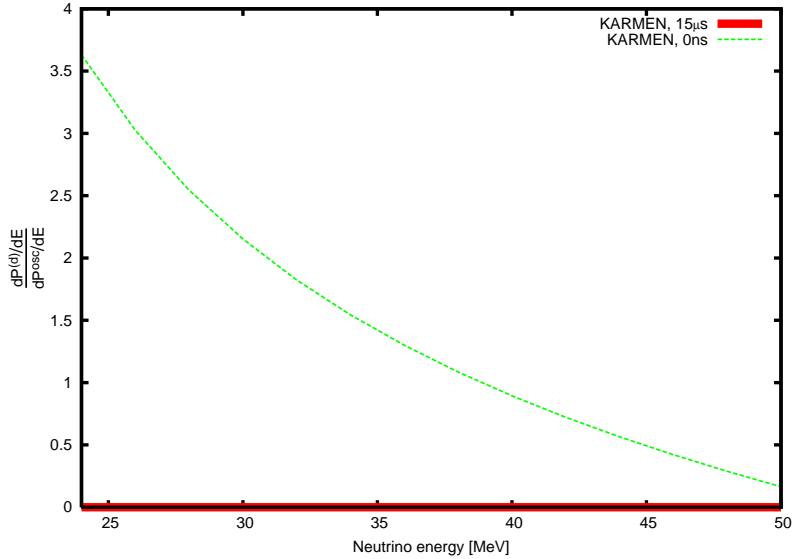


FIG. 12. (Color online) The Δt dependence of the ratio for KARMEN. $\Delta t = 0$ ns (green) and $\Delta t = 15\mu\text{s}$ (red). We used $m_{\nu_h} = 0.08$ eV of inverted hierarchy; all other parameters are the same as those in Fig. 11.

that of LSND.

Thus the difference between LSND and KARMEN results from the methods of the event selection, and an indication may appear as a sharp peak in the small Δt region in Ref. [33]. Accordingly, the experimental results of both LSND and KARMEN can be explained from $P^{(d)}$, and are consistent with the previous result of LSND πDIF [28]. With a precise energy spectrum and suitable selection criteria, it would be possible to confirm $P^{(d)}$ by the excess of $\bar{\nu}_e$ at near detector.

2. Future experiments of $\mu^+\text{DAR}$ and $\mu^+\text{DIF}$

There are two possible experiments to confirm $P^{(d)}$ from the excess of the neutrino flux. One is a $\bar{\nu}_e$ appearance experiment with $\mu^+\text{DAR}$ [34]; the other is a ν_μ appearance and $\bar{\nu}_\mu$ disappearance with $\mu^+\text{DIF}$ [35]. Here, we give predictions for future experiments regarding both cases.

1. $\mu^+\text{DAR}$

In $\mu^+\text{DAR}$ experiments, the $\bar{\nu}_e$ spectrum is given by Eq. (77). The ratio between $\bar{\nu}_e$ and

$\bar{\nu}_\mu$ spectra for events free from the double coincidence condition of Δt is written as

$$R_{\bar{\nu}_e}(E_\nu) = \frac{m_\mu^2 \sigma_{\bar{\nu}_e}}{8\pi} \frac{\left(1 - 2\frac{E_\nu}{m_\mu}\right) \left(5 - 6\frac{E_\nu}{m_\mu}\right)}{\left(3 - 4\frac{E_\nu}{m_\mu}\right) \left(e^{-\frac{T_\mu}{\tau_\mu}} - e^{-\frac{T_\mu+T_D}{\tau_\mu}}\right)} \tilde{g}_{\mu,e}(\omega_{\bar{\nu}_e}, T; \tau_\mu). \quad (79)$$

This is the value under ideal conditions. The value for an experimental setup [34] is shown in Fig. 13, where cT , the size of the beam stop, is 1 m, $T_\mu = 1 \mu\text{s}$, $cT_D = 3.4$ m, and $\sigma_{\bar{\nu}_e}$ is of $C_{2n}H_{2n+2}$ in the liquid scintillator. The ratio from the flavor oscillation with one sterile neutrino is, $\frac{dP^d/dE}{dP^{\text{osc}}/dE}$,

$$R_{\bar{\nu}_e}^{\text{osc}}(E_\nu) = \frac{m_\mu^2 \sigma_{\bar{\nu}_e}}{8\pi} \frac{\left(1 - 2\frac{E_\nu}{m_\mu}\right) \left(5 - 6\frac{E_\nu}{m_\mu}\right) \tilde{g}_{\mu,e}(\omega_{\bar{\nu}_e}, T; \tau_\mu)}{\left(3 - 4\frac{E_\nu}{m_\mu}\right) \left(e^{-\frac{T_\mu}{\tau_\mu}} - e^{-\frac{T_\mu+T_D}{\tau_\mu}}\right) \sin^2 2\theta_{\mu e} \sin^2 \left(1.27 \frac{\Delta m_{41}^2}{E_\nu} L\right)}. \quad (80)$$

Figure 14 shows the ratio in Eq. (80), where the experimental parameters are the same as those in Fig. (13) and the parameters of the sterile neutrino are [30]

$$\Delta m_{41}^2 = 0.9 \text{ eV}^2, \quad U_{e4} = 0.15, \quad U_{\mu4} = 0.17, \quad (81)$$

$$\sin^2 \theta_{\mu e} = 4 |U_{\mu4} U_{e4}|^2, \quad \sin^2 \theta_{\mu\mu} = 4 |U_{\mu4}|^2 (1 - |U_{\mu4}|^2). \quad (82)$$

These values are also used in the next μ^+ DIF case. According to Figs. 13 and 14, the magnitude of the $\bar{\nu}_e$ appearance through $P^{(d)}$ can be almost the same as, or larger than, that of the flavor oscillation with the sterile neutrinos. Furthermore, the effect is sensitive to the absolute neutrino mass and the mass hierarchy of the neutrino.

2. μ^+ DIF

In the μ^+ DIF experiment, an appearance of ν_μ ($\nu_e \rightarrow \nu_\mu$) from ν_e and a disappearance of $\bar{\nu}_\mu$ ($\bar{\nu}_\mu \rightarrow \bar{\nu}_e$) will be searched, as the flavor oscillations with sterile neutrinos are considered. The finite-size corrections provide the appearance of ν_μ and $\bar{\nu}_\mu$, but their magnitudes and spectra are very different from those of the sterile neutrinos. Using Eqs. (68) – (71), the ratios $\frac{P_{\nu_\mu}^{(d)}(E_\nu)}{P_{\nu_\mu}^{\text{osc}}(E_\nu)}$ and $\frac{P_{\bar{\nu}_\mu}^{(d)}(E_\nu)}{P_{\bar{\nu}_\mu}^{\text{osc}}(E_\nu)}$ are written as

$$R_{\nu_\mu}(E_\nu, \cos \theta) = \frac{\sigma_{\nu_\mu} (m_\mu^2 - 2E_\nu(E_\mu - p_\mu \cos \theta)) \tilde{g}_{e,\mu}(\omega_\nu, T; \gamma\tau_\mu)}{2\pi \left(\exp \left[-\frac{T_\mu}{\gamma\tau_\mu} \right] - \exp \left[-\frac{T_\mu+T}{\gamma\tau_\mu} \right] \right) \sin^2 2\theta_{\mu e} \sin^2 \left(1.27 \frac{\Delta m_{41}^2}{E_\nu} L \right)}, \quad (83)$$

$$R_{\bar{\nu}_\mu}(E_\nu, \cos \theta) = \frac{\sigma_{\bar{\nu}_\mu} (m_\mu^2 - 2E_\nu(E_\mu - p_\mu \cos \theta)) \tilde{g}_{e,\mu}(\omega_\nu, T; \gamma\tau_\mu)}{2\pi \left(\exp \left[-\frac{T_\mu}{\gamma\tau_\mu} \right] - \exp \left[-\frac{T_\mu+T}{\gamma\tau_\mu} \right] \right) \left(1 - \sin^2 2\theta_{\mu\mu} \sin^2 \left(1.27 \frac{\Delta m_{41}^2}{E_\nu} L \right) \right)}, \quad (84)$$

and that of $\bar{\nu}_\mu$ is given by Eq. (73). Eqs. (72) and (73) are given in Figs. 15 and 16. The target nucleus is ^{56}Fe and the parameters given in Eqs. (81) and (82) are used. The ratio

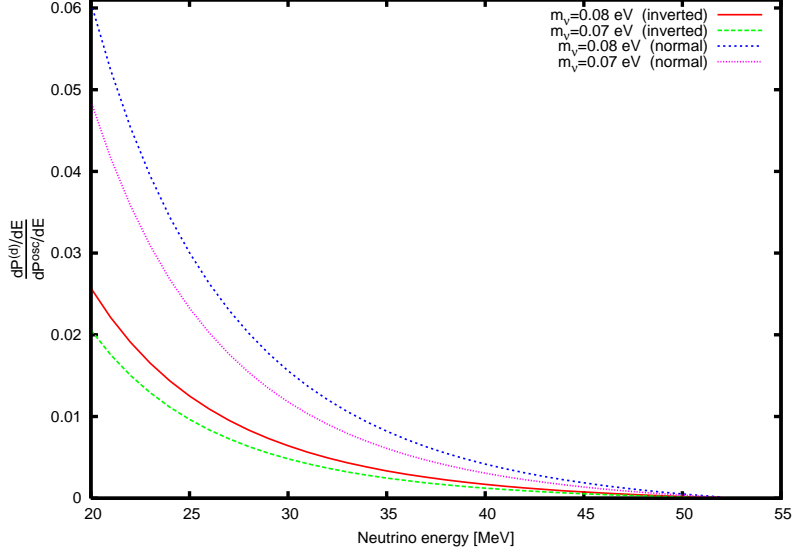


FIG. 13. (Color online) The ratios $\frac{dP_{\nu_e}^{(d)}/dE}{dP_{\nu_\mu}^{osc}/dE}$, Eq. (79), for μ^+ DAR are shown, where $T_\mu = 1 \mu\text{s}$, $cT = 1.0 \text{ m}$, $L = 17.0\text{m}$, and $\sigma_{\bar{\nu}_e} = 7.3$ of $C_{2n}H_{2n+2}$ and $cT_D = 3.4 \text{ m}$ are used [34]. The red curve shows the inverted hierarchy of $m_{\nu_h} = 0.08 \text{ eV}$, the green curve shows the inverted hierarchy of $m_{\nu_h} = 0.07 \text{ eV}$, the blue curve shows the normal hierarchy of $m_{\nu_h} = 0.08 \text{ eV}$, and the magenta curve shows the normal hierarchy of $m_{\nu_h} = 0.07 \text{ eV}$.

of ν_μ appearance at $L = 20 \text{ m}$ is very large. This is because T dependences are different in normal and diffraction terms. The normal term is very small at $T \ll \gamma\tau_\mu$ and P^0 increases with T , but the diffraction term $P^{(d)}$ is constant in T . In addition, the oscillation length with $\Delta m_{41}^2 = 0.9 \text{ eV}^2$ at $E_\nu = 1 \text{ GeV}$ is 800–900 m, and the effect of the flavor oscillation is not significant at $L = 20 \text{ m}$. Thus, the 10^3 larger magnitude of the ν_μ appearance through the finite-size correction at $L = 20 \text{ m}$ is a natural consequence of the nature of the diffraction term. Then, the relative magnitude between them becomes very large, of the order of 10^3 , at $cT = 226 \text{ m} \ll \gamma\tau_\mu$ at $E_\mu = 3 \text{ GeV}$.

The ratio of the ν_μ appearance at $L = 2000 \text{ m}$ has three peaks because the numerator $dP_{\nu_\mu}^{(d)}/dE_\nu$ varies uniformly in energy and the denominator $dP_{\nu_\mu}^{osc}/dE_\nu$ oscillates in energy, becoming very small at certain energies.

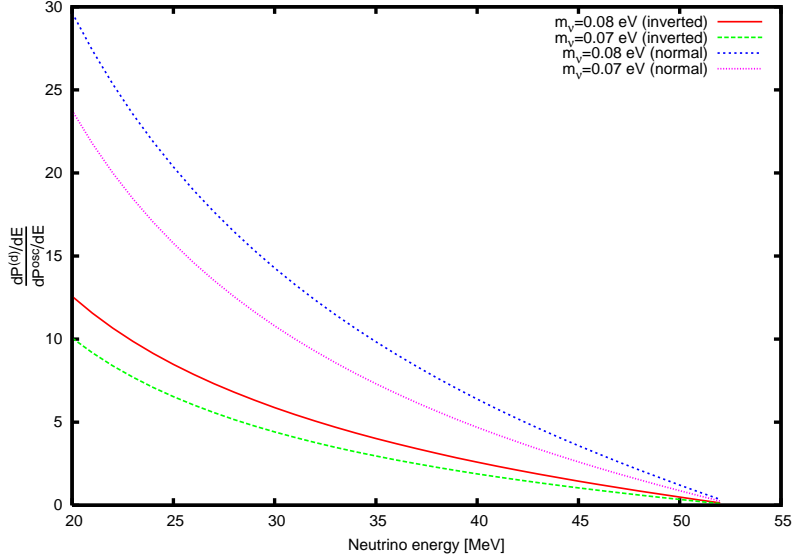


FIG. 14. (Color online) The ratios $\frac{dP_{\bar{\nu}_e}^{(d)}/dE}{dP_{\bar{\nu}_e}^{osc}/dE}$, Eq. (80), for μ^+ DAR are shown, where $T_\mu = 1 \mu\text{s}$, $cT = 1.0 \text{ m}$, $L = 17.0 \text{ m}$, $cT_D = 3.4 \text{ m}$, and $\sigma_{\bar{\nu}_e} = 7.3$ of $C_{2n}H_{2n+2}$ and are used [34]. The red curve shows the ratio of the inverted hierarchy with $m_{\nu_h} = 0.08 \text{ eV}$, the green curve shows that of the inverted hierarchy with $m_{\nu_h} = 0.07 \text{ eV}$, the blue curve shows the ratio of the normal hierarchy with $m_{\nu_h} = 0.08 \text{ eV}$, and the magenta curve shows the ratio of the normal hierarchy with $m_{\nu_h} = 0.07 \text{ eV}$.

D. Comparison of the flavor-changing probability with the flavor oscillation

$\tilde{g}_{\alpha\beta}(\omega_\nu, T, \tau_\mu)$ for $\alpha \neq \beta$ is approximately proportional to $\omega_\nu T$, whereas that of the single-particle formula is proportional to $(\omega_{\nu_i} - \omega_{\nu_j})^2 T^2$. Accordingly LSND data is explained using the single-particle formula of $\Delta m^2 \approx 1 \text{ eV}^2$, or using $P^{(d)}$ of much smaller masses of the standard three neutrinos. From $P^{(d)}$, excesses of $\bar{\nu}_\mu$ and ν_μ arise in μ^+ DIF, but that is not the case from the Γ . The two mechanisms can be clearly distinguished.

E. Modified survival probability due to $P^{(d)}$

For the neutrino, $\tau_\mu \ll T_0$, and the life-time effect was dominant in $t < \tau_\mu$. For the electron, ω_e is substantially larger and $T_0(e) \ll \tau_\mu$, and the effect due to $P_e^{(d)}$ appears before τ_μ . The survival probability has a contribution from $P_e^{(d)}$ in addition to ΓT ; the final value

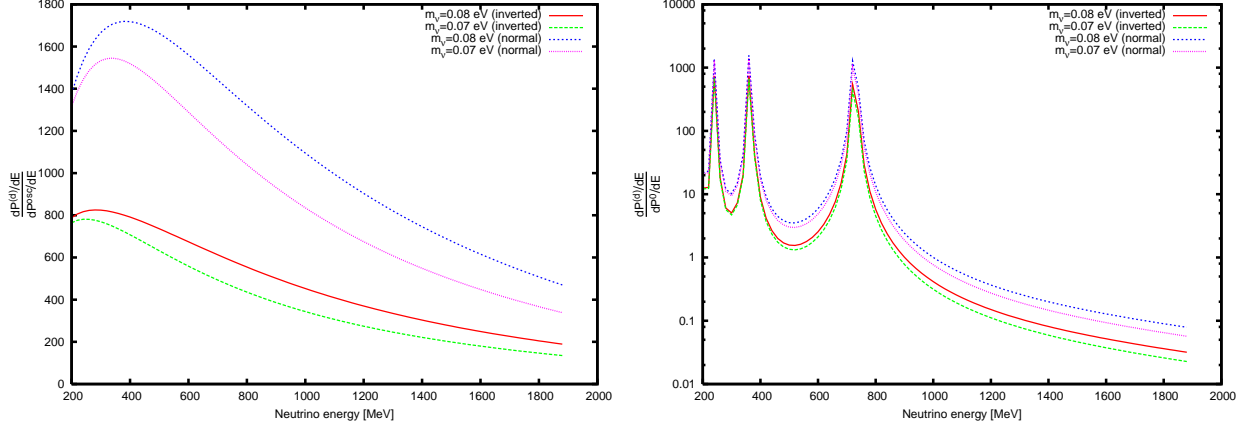


FIG. 15. (Color online) Ratios of ν_μ appearance $\frac{dP_{\nu\mu}^{(d)}/dE_\nu}{dP_{\nu\mu}^{osc}/dE_\nu}$, Eq. (80), for μ^+ DIF, where $T_\mu = 0$ μ s, $cT = 226.0$ m, $L = 20.0$ m (left) and $L = 2000.0$ m (right), and σ_{ν_μ} = of ^{56}Fe and $\cos\theta = 1$ are used [35]. The red curve shows the ratio of the inverted hierarchy with $m_{\nu_h} = 0.08$ eV, the green curve shows the ratio of the inverted hierarchy with $m_{\nu_h} = 0.07$ eV, the blue curve shows the ratio of the normal hierarchy with $m_{\nu_h} = 0.08$ eV, and the magenta curve shows the ratio of the normal hierarchy with $m_{\nu_h} = 0.07$ eV. In the right figure, there are three sharp peaks because the denominator oscillates in energy and becomes very small.

is given by

$$P_e^{\text{new}}(T) = \frac{1}{1 + P_e^{(d)}} e^{-\frac{T}{\tau_\mu}}. \quad (85)$$

$P_e^{(d)}$ becomes sizable for $\sigma_e \rightarrow \infty$, and the correction due to $P_e^{(d)}$ becomes then important.

IV. SUMMARY

It was found that the neutrinos in the wave zone participate in the muon decays. The transition probability at T is modified from the golden rule to $\Gamma T + P^{(d)}$. $P^{(d)}$ has the form Eq.(16), and shows the rapid transition at small T . These neutrinos reveal exciting behaviors within the standard model of three neutrino flavor. They are able to resolve the discrepancies among the neutrino experiments in short-distance region, and to provide the information on the neutrino absolute mass. $P^{(d)}$ is due to the non-stationary states of the overlapping initial and final waves, which extend to the macroscopic length L_c . L_c is inversely proportional to the neutrino mass-squared, and is much longer than the detector size. These states in the wave zone have the continuous spectrum of the kinetic energy which includes $\Delta E \rightarrow \infty$ in

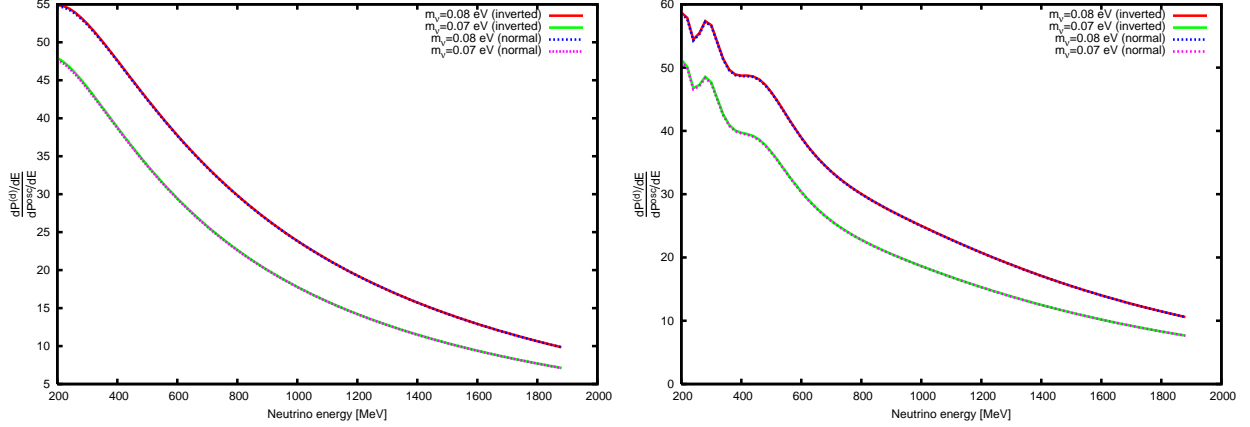


FIG. 16. (Color online) Ratios of excess and disappearance of $\bar{\nu}_\mu$, $\frac{dP_{\bar{\nu}_\mu}^{(d)}/dE}{dP_{\bar{\nu}_\mu}^{osc}/dE}$, Eq. (80), for μ^+ DIF, where $T_\mu = 0 \mu s$, $cT = 226.0$ m, $L = 20$ m (Left) and $L = 2000$ m (Right), and $\sigma_{\bar{\nu}_\mu} =$ of ^{56}Fe and $\cos \theta = 1$ are used [35]. The red curve shows the ratio of the inverted hierarchy with $m_{\nu_h} = 0.08$ eV, the green curve shows the ratio of the inverted hierarchy with $m_{\nu_h} = 0.07$ eV, the blue curve shows the ratio of the normal hierarchy with $m_{\nu_h} = 0.08$ eV, and the magenta curve shows the ratio of the normal hierarchy with $m_{\nu_h} = 0.07$ eV.

Eq.(5). Accordingly $P^{(d)}$ which rises steeply in small T becomes constant in large T . $P^{(d)}$ for the neutrino $P_\nu^{(d)}$ has the same expression with that of the electron $P_e^{(d)}$, but $P_\nu^{(d)} \gg P_e^{(d)}$ because $\frac{m_\nu}{m_e} \ll 1$. For the electron, the spectrum at T is expressed by the golden rule, and the probability that the electron is detected is in agreement with the probability that the muon has decayed. However for the neutrino, that is expressed by the sum of the terms from the golden rule and its correction, and depends on the initial state and the final state.

Since L_c is much longer than the detector size, the probability amplitude defined by the FQM between the non-stationary states and the outgoing states is necessary sensitive to the latter wavefunctions. The final states depend on the cut on the time difference Δt of the detection method. For the case of no cut, these are extended in large area in the configuration space and overlap with the initial state. For the case of the cut of a small Δt , a small portion of the wavefunction is excluded, and for that of a large Δt , a large portion of the wavefunction is excluded. Consequently $P^{(d)}$ is large for the case of no cut, but small for the case of large Δt . The analysis on the experiments is altered by $P^{(d)}$. The LSND, MiniBooNE, and KARMEN experiments have different geometries and used different Δt . Their $P^{(d)}$ are thus different. Surprisingly, the experiments seemingly

inconsistent with each other if the probability by the Fermi's golden rule, Γ , is used become consistent when $\Gamma T + P^{(d)}$ is used. In the geometry of long-distance oscillation experiments, $P^{(d)}$ is negligible [5], and the neutrino oscillations are described by the standard formula. Therefore, the neutrino oscillation experiments are in agreement with each other and with the theory within the three flavors, when the probability $\Gamma T + P^{(d)}$ is used. By measuring $P^{(d)}$ accurately, the absolute neutrino masses will be determined. The effects studied here are not modified by higher-order corrections.

The rigorous transition probability at T is derived from FQM and describes transitions in other systems of light particles as well. $P^{(d)}$ of intriguing properties appears in many transitions involving light particles, and gives sizable effects. They will be presented in separate publications.

ACKNOWLEDGMENTS

This work was partially supported by a Grant-in-Aid for Scientific Research (Grant No. 24340043). Authors thank Dr. Kobayashi, Dr. Maruyama, Dr. Suekane, Dr. Nakaya for useful discussions on the neutrino experiments, Dr. Asai, Dr. Kobayashi, Dr. Mori, Dr. Minowa, Dr. Yamada, Dr. Sloan, Dr. Arai, and Dr. Ojima, for useful discussions on quantum interferences.

Appendix A: Normal term

In $T \ll \tau_\mu$ the muon lifetime can be ignored, but in $T \approx \tau_\mu$, that cannot. In both cases, we have

$$\begin{aligned}
|I^{\text{normal}}(\delta p)|^2 &= \left(\frac{2\pi\sigma_\mu\sigma_{\nu_e}}{\sigma_\mu + \sigma_{\nu_e}} \right)^3 \exp \left[-\frac{\sigma_\mu\sigma_{\nu_e}}{(\sigma_\mu + \sigma_{\nu_e})} \delta\vec{p}^2 - \frac{(\vec{X}_\mu - \vec{X}_{\nu_e})^2}{(\sigma_\mu + \sigma_{\nu_e})} \right] \\
&\times \int dt_1 dt_2 e^{-\frac{t_1+t_2}{\tau_\mu} + i(\delta p^0 - \vec{v}_0 \cdot \delta\vec{p})(t_1 - t_2)} \\
&\times \exp \left[\frac{(\vec{v}_{\nu_e} - \vec{v}_\mu) \cdot (\vec{X}_{\nu_e} - \vec{X}_\mu)}{\sigma_\mu + \sigma_{\nu_e}} (t_1 + t_2) - \frac{(\vec{v}_{\nu_e} - \vec{v}_\mu)^2}{2(\sigma_\mu + \sigma_{\nu_e})} (t_1^2 + t_2^2) \right]. \quad (\text{A1})
\end{aligned}$$

Integrating over \vec{X}_{ν_e} ,

$$\int d\vec{X}_{\nu_e} |I^{\text{normal}}(\delta p)|^2 = 16 \frac{\pi^5 (\sigma_\mu \sigma_{\nu_e})^{\frac{3}{2}}}{(\sigma_\mu + \sigma_{\nu_e}) |\vec{v}_{\nu_e} - \vec{v}_\mu|} \exp \left[-\frac{\sigma_\mu + \sigma_{\nu_e}}{(\vec{v}_{\nu_e} - \vec{v}_\mu)^2} (\delta p^0 - \vec{v}_0 \cdot \delta \vec{p})^2 \right] \\ \times \exp \left[-\frac{\sigma_\mu \sigma_{\nu_e}}{\sigma_\mu + \sigma_{\nu_e}} \delta \vec{p}^2 \right] \frac{\tau_\mu}{2} \left(1 - e^{-\frac{2T}{\tau_\mu}} \right), \quad (\text{A2})$$

for the wave packets of $\sqrt{\frac{\sigma_\mu + \sigma_{\nu_e}}{(\vec{v}_\mu - \vec{v}_{\nu_e})^2}} \ll \tau_\mu, T$, and outside the probabilities from the normal term are computed numerically. For $T \ll \tau_\mu$, $\frac{\tau_\mu}{2} (1 - e^{-\frac{2T}{\tau_\mu}}) = T$.

Appendix B: Light-cone singularity

The light-cone singularities are explained in many textbooks and in Ref. [4, 5]; the new formulae used in this paper are briefly summarized.

(1) $D^+(\delta t, \delta \vec{x}; m)$ and $D^+(\delta t, \delta \vec{x}; im)$ are single particle correlation functions of the real mass and imaginary mass.

(2) The correlation function $D^+(\delta t, \delta \vec{x}; p, m)$ of an external momentum \mathbf{p} is written as $D^+(\delta t, \delta \vec{x}; p, m) = e^{-ip \cdot \delta x} D^+(\delta t, \delta \vec{x}, m)$, $p^2 = m_0^2$ or $D^+(\delta t, \delta \vec{x}; p, m) = D_\infty^+(\delta t, \delta \vec{x}; p, m) + D_{\text{finite}}^+(\delta t, \delta \vec{x}; p, m)$. The latter is written further

$$D_\infty^+(\delta t, \delta \vec{x}; p, m) = D_m(\xi) D_\infty^+(\delta t, \delta \vec{x}; i\tilde{m}), \quad (\text{B1})$$

$$\tilde{m} = \sqrt{m_0^2 - m^2}, \quad \xi = -2ip \cdot \frac{\partial}{\partial \delta x}, \quad D_m(\xi) = \sum_{l=0} \frac{\xi^l}{l!} \left(\frac{\partial}{\partial \tilde{m}^2} \right)^l,$$

$$D_m(\xi) D_\infty^+(\delta t, \delta \vec{x}; i\tilde{m}) = \frac{\epsilon(\delta t)}{4\pi} \delta(\lambda) + D_m(\xi) \left[-\frac{\tilde{m}}{8\pi\sqrt{-\lambda}} \theta(-\lambda) \left\{ N_1(\tilde{m}\sqrt{-\lambda}) \right. \right. \\ \left. \left. - i\epsilon(\delta t) J_1(\tilde{m}\sqrt{-\lambda}) \right\} + \theta(\lambda) \frac{\tilde{m}}{4\pi^2\sqrt{\lambda}} K_1(\tilde{m}\sqrt{\lambda}) \right]. \quad (\text{B2})$$

The light-cone singularity of $D_\infty^+(\delta t, \delta \vec{x}; p, m)$ is independent of p and m , and exists in the region expressed by Eq. (43) in the text.

The integral over the region $-p_0 \leq r_0 \leq 0$ is written as,

$$D_{\text{finite}}^+(\delta t, \delta \vec{x}; p, m) = \frac{1}{i(2\pi)^3} \int \frac{d\vec{q}}{E(\vec{q})} e^{i(q-p) \cdot \delta x} \theta(p_0 - E(\vec{q})). \quad (\text{B3})$$

For $\tilde{m}^2 < 0$, $D^+(\delta t, \delta \vec{x}; p, m) = 0$.

(3) $D^+(\delta t, \delta \vec{x}; p, m)_{\alpha_1, \alpha_2, \dots}$ of many-body states are expressed with the mass spectrum, $\rho(m^2)$, as

$$\int dm^2 \rho(m^2) D^+(\delta t, \delta \vec{x}; p, m), \quad (\text{B4})$$

$$\rho(m^2) = \int d(\text{phase space}) \delta \left(m^2 - \left(\sum_l p_l \right)^2 \right).$$

For two particles

$$\Delta_{e, \nu_\mu}(\delta x) = \frac{1}{(2\pi)^6} \int_{-\infty}^{\infty} \frac{d\vec{p}_e d\vec{p}_{\nu_\mu}}{E_e E_{\nu_\mu}} (p_\mu \cdot p_{\nu_e}) (p_e \cdot p_{\nu_\mu}) e^{i(p_e + p_{\nu_\mu} - p_\mu) \cdot \delta x}, \quad (\text{B5})$$

$$= \frac{p_\mu \cdot p_{\nu_e}}{2(2\pi)^2} \int dm^2 \left(m^2 - 2m_e^2 + \frac{m_e^4}{m^2} \right) i D^+(\delta t, \delta \vec{x}; p_\mu, m).$$

$$\Delta_{\nu_\mu, \nu_e}(\delta x) = \frac{1}{(2\pi)^6} \int_{-\infty}^{\infty} \frac{d\vec{p}_{\nu_\mu} d\vec{p}_{\nu_e}}{E_{\nu_\mu} E_{\nu_e}} (p_\mu \cdot p_{\nu_e}) (p_e \cdot p_{\nu_\mu}) e^{i(p_{\nu_\mu} + p_{\nu_e} - p_\mu) \cdot \delta x}, \quad (\text{B6})$$

$$= \frac{i}{12(2\pi)^2} \int dm^2 \left(m^2 (p_\mu \cdot p_e) + 2p_\mu \cdot \left(p_\mu - i \frac{\partial}{\partial \delta x} \right) p_e \cdot \left(p_\mu - i \frac{\partial}{\partial \delta x} \right) \right) \times D^+(\delta t, \delta \vec{x}; p_\mu, m). \quad (\text{B7})$$

Appendix C: Universal function $\tilde{g}(\omega, T; \tau_\mu)$

1. Asymptotic behaviors of integrals

The constant term of the integral over times plays a crucial role. First we study an integral of a function $f(t)$ of the property,

$$\mathcal{I}(T) = \int_0^T dt_1 \int_0^T dt_2 f(t_1 - t_2) = CT + I_0, \quad (\text{C1})$$

for a large T and evaluate the constants C and I_0 . For a short-range function $f(t)$ that decreases rapidly and is negligible in $|t| \geq \epsilon$, the integral for $T \gg \epsilon$,

$$\mathcal{I}(T) = \int_{0+\epsilon}^{T-\epsilon} dt_1 \int_0^T dt_2 f(t_1 - t_2) + \epsilon \left(\int_0^T dt_1 (f(T - t_1) + f(t_1 - T)) \right) = C(T - \epsilon), \quad (\text{C2})$$

$$C = \int_{-\infty}^{\infty} dt f(t), I_0 = -\epsilon C.$$

Thus I_0 is negligible for a microscopic ϵ .

I_0 is significant only for a macroscopic ϵ or for a long-range $f(t)$. One example is

$$Tg(\omega T) = \int_0^T dt_1 \int_0^T dt_2 \frac{\sin(\omega_\nu(t_1 - t_2))}{t_1 - t_2} = T\pi + T\tilde{g}(\omega_\nu T), \quad (\text{C3})$$

where $T\tilde{g}(\omega_\nu T)$ was given in [4] and in Eq.(C13), and is not negligible.

From Eq.(34), the probability is expressed with the integral over the coordinates x_1, x_2 , and \vec{X}_{ν_e}

$$\begin{aligned}
I(T) &= \int d\vec{X}_{\nu_e} \int d^4x_1 d^4x_2 e^{ip_{\nu_e} \cdot \delta x} f(\delta x) \prod_{i=1,2} w(x_i, X_\mu; \sigma_\mu) w(x_i, X_{\nu_e}; \sigma_{\nu_e}) \\
&= \left(\frac{\pi \sigma_\mu \sigma_{\nu_e}}{\sigma_\mu + \sigma_{\nu_e}} \right)^{\frac{3}{2}} \int d\vec{X}_{\nu_e} e^{-\frac{(\vec{X}_\mu - \vec{X}_{\nu_e})^2}{\sigma_\mu + \sigma_{\nu_e}} T} \int dt_1 dt_2 d\delta\vec{x} e^{ip_{\nu_e} \cdot \delta x} e^{-\frac{1}{4\sigma_\mu} (\delta\vec{x} - \vec{v}_\mu \delta t)^2 - \frac{1}{4\sigma_{\nu_e}} (\delta\vec{x} - \vec{v}_{\nu_e} \delta t)^2} \\
&\times e^{-\frac{t_1+t_2}{\tau_\mu}} \exp \left[-\frac{(\vec{v}_\mu - \vec{v}_{\nu_e})^2}{\sigma_\mu + \sigma_{\nu_e}} \left(\frac{t_1 + t_2}{2} - \tilde{T}_L \right)^2 \right] f(\delta x), \tag{C4} \\
\tilde{T}_L &= \frac{(\vec{v}_\mu - \vec{v}_{\nu_e}) \cdot (\vec{X}_\mu - \vec{X}_{\nu_e})}{(\vec{v}_\mu - \vec{v}_{\nu_e})^2},
\end{aligned}$$

where $f(\delta x)$ is derived from the correlation function. This is reduced to an integral of the form of Eq.(C1) using a Gaussian approximation for the integration in \vec{X}_{ν_e} ,

$$I(T) = (\pi^2 \sigma_\mu \sigma_{\nu_e})^{\frac{3}{2}} \int_0^T dt_1 \int_0^T dt_2 d\delta\vec{x} e^{ip_{\nu_e} \cdot \delta x} e^{-\frac{1}{4\sigma_\mu} (\delta\vec{x} - \vec{v}_\mu \delta t)^2 - \frac{1}{4\sigma_{\nu_e}} (\delta\vec{x} - \vec{v}_{\nu_e} \delta t)^2} e^{-\frac{t_1+t_2}{2\tau_\mu}} f(\delta x). \tag{C5}$$

Eq.(C5) for $f(x) = D^+(\delta t, \delta\vec{x}; p_\mu, m)^{(1)}$ or $f(x) = D^+(\delta t, \delta\vec{x}; p_\mu, m)^{(3)}$ is short-range in $t_1 - t_2$ and $I(T)$ is proportional to T . Now for $f(\delta x) = i \frac{\epsilon(\delta t)}{4\pi} \delta(\lambda)$,

$$I(T) \simeq \int_0^T dt_1 \int_0^T dt_2 (\pi^2 \sigma_\mu \sigma_{\nu_e})^{\frac{3}{2}} \frac{i}{2} \sigma_{\nu_e} e^{-\frac{(\vec{v}_\mu - \vec{v}_{\nu_e})^2}{4\sigma_\mu} \delta t^2} e^{-\frac{(1-|\vec{v}_{\nu_e}|)^2}{4\sigma_{\nu_e}} \delta t^2} \frac{e^{i\omega_{\nu_e} \delta t}}{\delta t} e^{-\frac{t_1+t_2}{2\tau_\mu}}, \tag{C6}$$

has both components and $I(T) = CT + I_0$, where $\omega_{\nu_e} = \frac{m_{\nu_e}^2}{2E_{\nu_e}}$, and $\sigma_{\nu_e} |\vec{p}_{\nu_e}| \ll T$ is used. Owing to the small mass of the neutrino, $e^{-\frac{(1-|\vec{v}_{\nu_e}|)^2}{4\sigma_{\nu_e}} \delta t^2} \approx 1$. For the case $\frac{(\vec{v}_\mu - \vec{v}_{\nu_e})^2}{4\sigma_\mu} T^2 \ll 1$, that is reduced to the integral

$$\tau_\mu g(\omega_\nu, T; \tau_\mu) = -\tau_\mu \int_0^T dt \frac{\sin(\omega_\nu t)}{t} \left(e^{-\frac{t}{2\tau_\mu}} - e^{-\frac{1}{2\tau_\mu} (2T-t)} \right), \tag{C7}$$

which is an extended version of the function Eq.(C3). For $\tau_\mu = \infty$, the constant term in $Tg(\omega_\nu, T; \tau_\mu)$ is obtained from $T\tilde{g}(\omega_\nu T)$. For finite τ_μ , that varies depending on the relative magnitudes of τ_μ and $T_0 = \frac{1}{\omega_\nu}$. The constant term of $g(\omega_\nu, T; \tau_\mu)$ is expressed differently.

1. $\tau_\mu \gg T_0$. In this case, $g(\omega_\nu, t; \tau_\mu)$ at $t < T_0$ is equivalent to $g(\omega_\nu, t; \infty)$. Its short-range component is combined with the short-range terms from $D^+(\delta t, \delta\vec{x}; p_\mu, m)^{(1)}$ and $D^+(\delta t, \delta\vec{x}; p_\mu, m)^{(3)}$. The rest $\tilde{g}^{(1)}(\omega_\nu, T; \tau_\mu) = g(\omega_\nu, T; \tau_\mu) - g(\omega_\nu, \infty; \infty)$, determines the constant term.

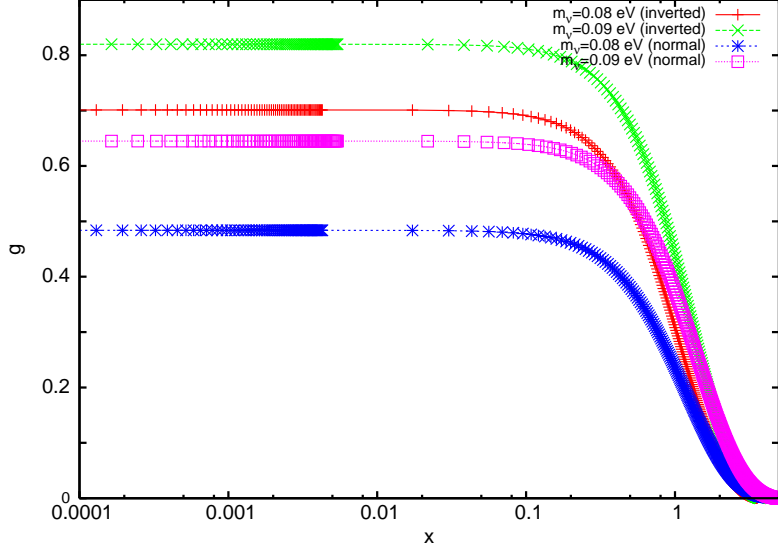


FIG. 17. (Color online) $\tilde{g}_{e,e}(\omega_{\nu_e}, T; \tau_\mu)$ including the flavor mixing, Eq. (C11). The horizontal axis is $x = \omega_{\nu_h} T$, where $\omega_{\nu_h} = \frac{m_{\nu_h}^2}{2E_{\nu_e}}$, m_{ν_h} is the mass of the heaviest neutrino. The different colors indicate different mass values of $m_{\nu_h} = 0.09$ eV (green: inverted hierarchy, magenta: normal hierarchy) and $m_{\nu_h} = 0.08$ eV (red: inverted hierarchy, blue: normal hierarchy).

2. $T_0 \gg \tau_\mu$. In this case, in $g(\omega_\nu, t; \tau_\mu)$ at $t < \tau_\mu$, the short-range component is expressed by $g(\omega_\nu, t = \infty; \tau_\mu)$, and is combined with the other short-range terms. The rest $\tilde{g}^{(2)}(\omega_\nu, T; \tau_\mu) = g(\omega_\nu, T; \tau_\mu) - g(\omega_\nu, \infty; \tau_\mu)$ determines the constant term. The neutrino masses around 0.08 eV correspond to the second case. Hereafter, we study the second case.

2. General form of $\tilde{g}(\omega_\nu, T; \tau_\mu)$

a. Without mixing

The universal function $\tilde{g}(\omega_\nu, T; \tau_\mu)$ is written from Eq.(C7) as

$$\tilde{g}(\omega_\nu, T; \tau_\mu) = \arctan(2\omega_\nu \tau_\mu) - \int_0^T dt \frac{\sin(\omega_\nu t)}{t} \left(e^{-\frac{t}{2\tau_\mu}} - e^{-\frac{1}{2\tau_\mu}(2T-t)} \right). \quad (\text{C8})$$

$$g(\omega_\nu, \infty; \tau_\mu) = -\arctan(2\omega_\nu \tau_\mu).$$

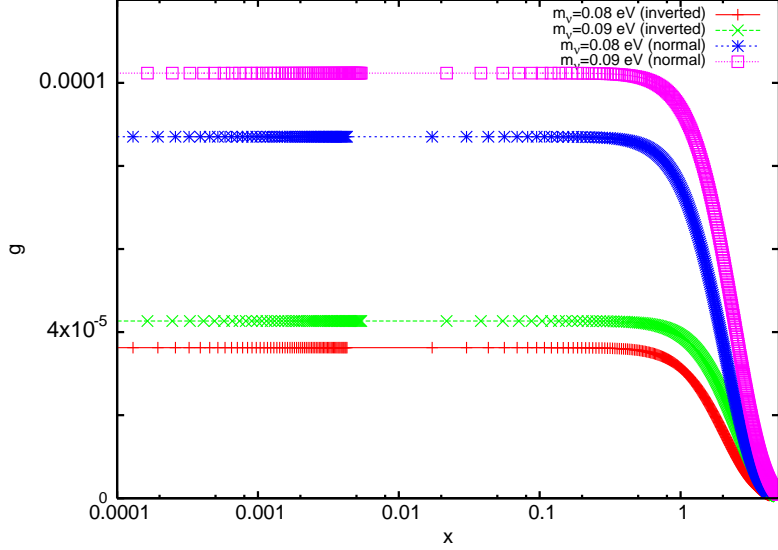


FIG. 18. (Color online) $\tilde{g}_{\mu,e}(\omega_{\nu_e}, T; \tau_\mu)$ including flavor mixing, Eq. (C11). The horizontal axis is $x = \omega_{\nu_h} T$, where $\omega_{\nu_h} = \frac{m_{\nu_h}^2}{2E_{\nu_e}}$, m_{ν_h} is the mass of the heaviest neutrino. Different colors represent different mass values of $m_{\nu_h} = 0.09$ eV (green: inverted hierarchy, magenta: normal hierarchy) and $m_{\nu_h} = 0.08$ eV (red: inverted hierarchy, blue: normal hierarchy).

b. Mixing case

$P^{(d)}$ in the system of the mixing is expressed with the integral for the mass eigenstates of m_i and m_j ,

$$\begin{aligned}
\mathcal{C}g(\omega_i, \omega_j, T; \tau_\mu) &= -\frac{\tau_\mu}{1 + \tau_\mu^2(\omega_i - \omega_j)^2} \int_0^T dt \frac{\sin\left(\left(\omega_i + \omega_j\right)\frac{t}{2}\right)}{t} \\
&\times \left[e^{-\frac{t}{2\tau_\mu}} \left\{ \cos\left(\left(\omega_i - \omega_j\right)\frac{t}{2}\right) - \tau_\mu(\omega_i - \omega_j) \sin\left(\left(\omega_i - \omega_j\right)\frac{t}{2}\right) \right\} \right. \\
&\left. - e^{-\frac{1}{2\tau_\mu}(2T-t)} \left\{ \cos\left(\left(\omega_i - \omega_j\right)\left(T - \frac{t}{2}\right)\right) - \tau_\mu(\omega_i - \omega_j) \sin\left(\left(\omega_i - \omega_j\right)\left(T - \frac{t}{2}\right)\right) \right\} \right], \tag{C9}
\end{aligned}$$

$$\begin{aligned}
\mathcal{C}g(\omega_i, \omega_j, \infty; \tau_\mu) &= \frac{\tau_\mu}{1 + \tau_\mu^2(\omega_i - \omega_j)^2} \left[-\frac{1}{2}(\arctan(2\omega_i\tau_\mu) + \arctan(2\omega_j\tau_\mu)) \right. \\
&\left. + \frac{\tau_\mu(\omega_i - \omega_j)}{4} [-\log(1 + 4\omega_j^2\tau_\mu^2) + \log(1 + 4\omega_i^2\tau_\mu^2)] \right]. \tag{C10}
\end{aligned}$$

This is combined with the mixing matrix and the universal function is written as

$$\tilde{g}_{\alpha,\beta}(\omega_{\nu_\beta}, T; \tau_\mu) = \sum_{i,j} U_{\beta,i} U_{\alpha,i}^* U_{\beta,j}^* U_{\alpha,j} (g(\omega_i, \omega_j, T; \tau_\mu) - g(\omega_i, \omega_j, \infty; \tau_\mu)), \quad (\text{C11})$$

and shown in Figs. 17 and 18 as a function of $x = \omega_\nu T$. According to those figures, $\tilde{g}_{\alpha,\beta}(\omega_{\nu_e}, T; \tau_\mu)$ is sensitive to the absolute neutrino mass and mass hierarchy, and causes the observable effects discussed in the text. The value of x is 0.0006 or 0.0007 for $cT = 1$ m, $m_{\nu_2} = 0.08$ eV, and $m_{\nu_2} = 0.09$ eV, and is 0.08 for $cT = 100$ m, $m_{\nu_2} = 0.08$ eV, and $m_{\nu_2} = 0.09$ eV; $\tilde{g}_{e,e}(\omega_{\nu_e})$ and $\tilde{g}_{\mu,e}(\omega_{\nu_e})$ are almost constant at $cT < 100$ m, but the magnitude is sensitive to the absolute neutrino mass. Thus, there is a wide window where the absolute neutrino mass can be measured by using the finite-size corrections. Furthermore, $\tilde{g}_{\mu,e}(\omega_{\nu_e})$ is considerably smaller than $\tilde{g}_{e,e}(\omega_{\nu_e})$, but does not vanish, and causes a new flavor changing effect on the neutrino.

3. Large life-time and T

For $\omega T \gg 1$, the universal function Eq. (C8) behaves as

$$\tilde{g}(\omega, T; \tau) \propto \frac{1}{\omega T}, \quad \omega \tau \approx 1 \quad (\text{C12})$$

$$\tilde{g}(\omega, T; \tau) \sim \frac{2}{\omega T}, \quad \tau \rightarrow \infty. \quad (\text{C13})$$

4. Angle dependence of overlapping region T

For μ^+ DAR, the region where parent and daughters overlap is sensitive to the geometry of the experiments, and the diffraction term depends on the angle between the beam axis and the detector, even if the decay is spherically symmetric. Following Fig. 19, the angle dependence region denoted as T in the text is written as

$$T = \begin{cases} \frac{2a}{\cos(\frac{\pi}{2}-\theta)} & \text{for } 0 \leq \cos \theta < \frac{b}{\sqrt{a^2+b^2}} \\ \frac{2b}{\cos \theta} & \text{for } \frac{b}{\sqrt{a^2+b^2}} \leq \cos \theta, \end{cases} \quad (\text{C14})$$

where θ is the angle between the beam axis and the detector, and a and b are the height and length of the detector, respectively. The probability of the event detected at the detector is averaged over the angle within the detector.

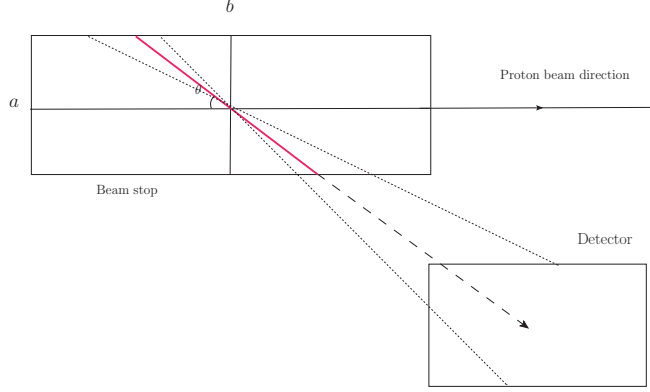


FIG. 19. (Color online) Angle dependence of the overlapping region (red line) for μ^+ DAR. It changes with the position and size of the detector.

5. σ_μ dependence

g for a finite σ_μ , which corresponds to μ^- DAR forming a bound state, is

$$\begin{aligned}
g(\omega_\nu, T; \tau_\mu) &= \int_{-T}^0 dt_- \int_{-\frac{1}{2}t_-}^{T+\frac{1}{2}t_-} dt_+ \frac{|\vec{v}_{\nu_e}| t_- \sin(\omega_{\nu_e} t_-)}{\vec{v}_{\nu_e}^2 t_-^2 + 4|\vec{p}_{\nu_e}|^2 \sigma_{\nu_e}^2} e^{-\frac{(\vec{v}_\mu - \vec{v}_{\nu_e})^2}{\sigma_\mu + \sigma_{\nu_e}} (t_+ - \tilde{T}_L)^2} e^{-\frac{2t_+}{\tau_\mu}} \\
&+ \int_0^T dt_- \int_{\frac{1}{2}t_-}^{T-\frac{1}{2}t_-} dt_+ \frac{|\vec{v}_{\nu_e}| t_- \sin(\omega_{\nu_e} t_-)}{\vec{v}_{\nu_e}^2 t_-^2 + 4|\vec{p}_{\nu_e}|^2 \sigma_{\nu_e}^2} e^{-\frac{(\vec{v}_\mu - \vec{v}_{\nu_e})^2}{\sigma_\mu + \sigma_{\nu_e}} (t_+ - \tilde{T}_L)^2} e^{-\frac{2t_+}{\tau_\mu}}, \\
t_+ &= \frac{t_1 + t_2}{2}, \quad t_- = t_1 - t_2.
\end{aligned}$$

For μ^+ DAR, μ^+ expands within the beam stop, while σ_μ almost does not change with T . Therefore, the σ_μ dependence can be included in the T -dependence. For μ^\pm DIF, σ_μ is determined by the coherence lengths of the parent particles, and is estimated as 0.1–1 m [5]. Then it is good to approximate the muon by a plane wave.

-
- [1] V. Weisskopf and E. Wigner, Z. Phys. **63**, 54 (1930).
 - [2] P. A. M. Dirac, Pro. R. Soc. Lond. **A 114**, 243-265, (1927).
 - [3] J. von Neumann, Mathematical Foundations of Quantum Mechanics (Princeton University Press, Princeton, 1955), p.290.
 - [4] K. Ishikawa and Y. Tobita, Prog. Theor. Exp. Phys. **2013**, 073B02 (2013).
 - [5] K. Ishikawa and Y. Tobita, Ann of Phys, **344**, 118 (2014).
 - [6] K. Ishikawa, T. Tajima, and Y. Tobita, Prog. Theor. Exp. Phys. **2015**, 013B02 (2015).

- [7] K. Ishikawa and Y. Tobita, “Finite-size corrections to Fermi’s golden rule II:Quasi-stationary composite states”, arXiv:1607.08522[hep-ph].
- [8] K. A. Olive et. al., (Particle Data Group), Chi. Phys. **C38**, 090001 (2014).
- [9] J.Schwinger,Phys. Rev. **74**,1439 (1948).
- [10] S.Tomonaga, Prog.Theor.Phys.**1**,27,(1946).
- [11] R. Feynman, Phys. Rev. **76**, 749 (1949).
- [12] M. L. Goldberger and K. M. Watson, Phys. Rev. **136**, 1472 (1964).
- [13] A. Einstein, B. Podlisky, and N. Rosen, Phys. Rev. **47**, 1777 (1935).
- [14] M. Gell-Mann, The Quark and the Jaguar: Adventures in the Simple and the Complex (St. Martin’s Griffin, London, 1995), ILL ed.
- [15] K. Ishikawa and T. Shimomura, Prog. Theor. Phys. **114**, 1201 (2005).
- [16] H. Lehman, K. Symanzik, and W. Zimmermann, Nuovo Cim. **1**, 205 (1955).
- [17] K. Ishikawa and Y. Tobita, Prog. Theor. Phys. **122**, 1111 (2009).
- [18] V. N. Aseev, et. al., Phys. Rev. D **84**, 112003 (2011).
- [19] E. Komatsu, et. al., Astrophys. J. Suppl., **192**, 18 (2011).
- [20] G. Hinshaw, et. al., arXiv:1212.5226 [astro-ph.CO].
- [21] P. A. R. Ade, et. al., arXiv:1303.5076 [astro-ph.CO].
- [22] K. Ishikawa and Y. Tobita, arXiv:1311.6917 [hep-ph].
- [23] R. Jost and H. Lehmann, Nuovo Cim. **5**, 1598 (1957).
- [24] F. J. Dyson, Phys. Rev. **110**, 1460 (1958).
- [25] C. Athanassopoulos, et. al. (LSND Collaboration), Phys. Rev. C **58**, 2489 (1998) .
- [26] A. Aguilar, et. al., Phys Rev. D **64**, 112007 (2001).
- [27] A. Aguilar, et. al., Annu.Rev .Nucl. Part. SCI.63,45(2013)
- [28] K. Ishikawa and Y. Tobita, arXiv:1209.5586 [hep-ph].
- [29] K. Abazajian, M. Acero, S. Agarwalla, A. Aguilar-Arevalo, C. Albright, et. al., (2012), arXiv:1204.5379 [hep-ph] and references therein.
- [30] J. Kopp, P. A. N. Machado, M. Maltoni, and T. Schwetz, JHEP 1305, 050 (2013).
- [31] A. A. Aguilar-Arevalo et. al., Phys. Rev. Lett. **110**, 161801 (2013).
- [32] Chen H, et. al. (MicroBooNE Collab.) Proposal for a New Experiment Using the Booster and NuMI Neutrino Beamlines. FERMILAB-PROPOSAL-0974. Batavia, Ill.: Fermi Natl. Accel. Lab. (2007); Chen H, et. al. (MicroBooNE Collab.) Addendum to Proposal for a New

Experiment Using the Booster and NuMI Neutrino Beamlines. Batavia, Ill.: Fermi Natl. Accel. Lab. (2008).

[33] B. Armbruster, et. al., Phys. Rev. D **65**, 112001 (2002).

[34] M. Harada, et. al., arXiv:1310.1437 [physics.ins-det].

[35] D. Adey, et. al., arXiv:1308.6822 [physics].